Time diminishing schemes (TDS) for kinetic equations in the diffusive scaling

Anaïs Crestetto* Nicolas Crouseilles† Giacomo Dimarco‡ Mohammed Lemou§

July 11, 2018

Abstract

In this work, we develop a new class of numerical schemes for collisional kinetic equations in the diffusive regime. The first step consists in reformulating the problem by decomposing the solution in the time evolution of an equilibrium state plus a perturbation. Then, the scheme combines a Monte Carlo solver for the perturbation with a Eulerian method for the equilibrium part, and is designed in such a way to be uniformly stable with respect to the diffusive scaling and to be consistent with the asymptotic diffusion equation. Moreover, since particles are only used to describe the perturbation part of the solution, the scheme becomes computationally less expensive - and is thus time diminishing (TDS) - as the solution approaches the equilibrium state due to the fact that the number of particles diminishes accordingly. This contrasts with standard methods for kinetic equations where the computational cost increases (or at least does not decrease) with the number of interactions. At the same time, the statistical error due to the Monte Carlo part of the solution decreases as the system approaches the equilibrium state: the method automatically degenerates to a solution of the macroscopic diffusion equation in the limit of infinite number of interactions. After a detailed description of the method, we perform several numerical tests and compare this new approach with classical numerical methods on various problems up to the full three dimensional case.

Mathematics Subject Classification: 65M06, 35B25, 82C80, 82D10, 41A60

Keywords: Kinetic equations; Diffusion scaling, Asymptotic preserving schemes; Time diminishing schemes; Micro-macro decomposition; Monte Carlo methods.

1 Introduction

Kinetic equations are commonly used to describe several phenomena arising in physics such as rarefied gas [5, 24], neutron transport [10], radiative transfer [11], plasmas [6] or electron flow in

[1]Laboratoire de Mathématiques Jean Leray, CNRS UMR 6629, Université de Nantes, France & INRIA Rennes - Bretagne Atlantique, MINGuS team. E-mail: anais.crestetto@univ-nantes.fr

[2]Univ Rennes & INRIA Rennes - Bretagne Atlantique, MINGuS team & Institut de Recherche Mathématiques de Rennes, CNRS UMR 6625, Université de Rennes 1, France & ENS Rennes. E-mail: nicolas.crouseilles@inria.fr

[3]Department of Mathematics and Computer Science. University of Ferrara, Italy. E-mail: giacomo.dimarco@unife.it

[4]Univ Rennes & Institut de Recherche Mathématiques de Rennes, CNRS UMR 6625, Université de Rennes 1, France & INRIA Rennes - Bretagne Atlantique, MINGuS team & ENS Rennes. E-mail: mohammed.lemou@univ-rennes1.fr

semiconductors [45]. In the description of these problems, one often encounters different spatio-temporal scales which are due to the coexistence of equilibrium and non equilibrium phenomena. This makes the problem hard to solve from the numerical point of view: the full kinetic model has to be considered everywhere to capture the correct physics. This means that the numerical method should deal with the high dimensionality issue and with different scales at the same time. Then, whenever a direct discretization is considered, strong constraints on the time step are required which involves huge computational cost. In addition, passing from the microscopic to the macroscopic description may change the nature of the equations and the numerical method should be able to follow this transition. This is the specific case considered in this work, in which equations pass from a hyperbolic to a parabolic structure [4]. Consequently, the characteristic speeds of the hyperbolic system grow to infinity as the scaling parameter tends to zero [4, 13] causing severe CFL restrictions in standard explicit numerical methods. Unfortunately, the alternative consisting in using macroscopic models can not be an option since macroscopic models are not able to capture non equilibrium effects. Thus, a natural idea consists in performing a domain decomposition approach and use the suitable model in the appropriate region [1, 2, 9, 21, 19, 18, 27, 29, 30, 32, 33, 34, 35, 43, 50]. This strategy is somehow optimal in terms of efficiency since the expensive kinetic model is used only when necessary, but it requires to connect the macro and micro models which is not an easy task at both mathematical and numerical levels, even if efficient approaches have been recently developed [26, 51]. Another way to handle such multiscale nature of the phenomena is to use asymptotic preserving methods [7, 8, 17, 25, 37, 28, 48, 31, 36, 39, 40, 41, 42, 46] which enable to overcome the numerical stiffness and to use time and space steps which are independent of the stiffness parameters which characterize the fast scales. However, while this approach permits to solve the problem related to the choice of the small time and space steps, it does not overcome the cost related to the solution of the kinetic model even in the equilibrium regions where a much less complex asymptotic model could be used.

In this work, we propose a numerical method which tries to take the best of the above two approaches: domain decomposition and asymptotic preservation. The method is based on a hybrid Monte Carlo strategy [12, 38] for the underlying kinetic equation which follows the ideas introduced in [23, 22, 20] and more recently in [16, 15, 14] in the context of gas dynamics. The problem addressed is the solution of a kinetic type equation under a diffusive scaling which in the limit gives rise to a parabolic type equation. More in details, the equation we consider is the following radiative transport equation (RTE)

$$\partial_t f + \frac{1}{\varepsilon}\mathbf{v}\cdot\nabla_{\mathbf{x}} f = \frac{1}{\varepsilon^2}(\rho M - f), \quad f(t=0,\mathbf{x},\mathbf{v}) = f_0(\mathbf{x},\mathbf{v}), \tag{1.1}$$

where $f(t,\mathbf{x},\mathbf{v})$ represents the density of particles in phase space with $\mathbf{x}\in\Omega\subset\mathbb{R}^{d_x}$, $\mathbf{v}\in V=\mathbb{R}^{d_v}$, $d_x\in\mathbb{N}^*$ is the dimension in space, $d_v\in\mathbb{N}^*$ in velocity space and ε the scaling parameter. The density $\rho(t,\mathbf{x})$ of the particles is given by

$$\rho(t,\mathbf{x}) = \int_V f(t,\mathbf{x},\mathbf{v})\mathrm{d}\mathbf{v}, \qquad \text{while} \qquad M(\mathbf{v}) = \frac{1}{(2\pi)^{d_v/2}}\exp\left(-\frac{|\mathbf{v}|^2}{2}\right) \tag{1.2}$$

is the so-called absolute Maxwellian. Finally $f_0(\mathbf{x},\mathbf{v})$ is a given initial condition and we consider periodic boundary conditions in space. To achieve our goal in this context, we proceed as follows: we couple a Monte Carlo method for the solution of the kinetic model with a finite volume method

for the solution of the macroscopic one [23, 22, 20]. However, instead of solving directly the kinetic model, we reformulate the original problem by using a micro-macro decomposition strategy [44, 42, 3, 17, 14, 15]. This permits to derive an equivalent set of equations which expresses the time evolution of the macroscopic part $\rho(t,\mathbf{x})M(\mathbf{v})$ plus the time evolution of the perturbation $g(t,\mathbf{x},\mathbf{v})$. Our strategy will be shown to have a low complexity in the fluid regions, which is comparable to that of domain decomposition methods in these regions. In other words, our method has almost a fluid complexity in the fluid regions. Moreover, our approach has even lower complexity in the kinetic regions compared to domain decomposition methods, since only the deviation from equilibrium has to be discretized with the Monte Carlo method, not the whole distribution f. Successively, we derive our numerical method by using an asymptotic preserving approach for the microscopic part of the solution which overcomes the parabolic stiffness and freezes the characteristic speeds in terms of the scaling parameter.

Since the kinetic equation which describes the evolution of the perturbation is solved by a particle approach, the result is a scheme in which the computational cost depends on the magnitude of the perturbation. The larger is the fraction of the solution far from equilibrium, the larger is the number of particles used. Moreover, since this fraction changes with time and space, the method automatically adapts itself to optimize the solution in terms of computational cost and reduction of the statistical error. In fact, the part of the solution described by particles is the lowest possible at each instant of time. This means that the proposed method realizes a variance reduction method whose effectiveness depends on the regime studied. As and where the equilibrium is approached, the number of particles in the Monte Carlo method is reduced, which decreases the computational cost enough to make it almost equivalent to the computational cost of a classical numerical method for the diffusion equation. Thus, the method realizes somehow an automatic domain decomposition method without imposing any artificial transition to pass from the microscopic to the macroscopic model. The transition only depends on the physics and not on numerical artifacts. Moreover, the computational cost continuously diminishes passing from one regime to the other. At the same time, with respect to standard AP schemes the reduction of the complexity is not only due to the overcoming of the stiffness of the collisional scale, but also to the reduction of the dimensionality of the problem in the diffusion asymptotics.

The rest of the paper is organized as follows. Section 2 is concerned with the presentation of the model, the derivation of the micro-macro equivalent model and its diffusion asymptotic. In Section 3 we present the asymptotically stable discretization of the microscopic model and a Monte Carlo Lagrangian discretization is proposed. In the same section, the discretization of the macroscopic part by a suitable Eulerian scheme that avoids the parabolic constraint on the time step is discussed. Section 4 is devoted to numerical results and analysis of the performances of the proposed method by treating problems from one up to three spatial dimensions. Finally, some remarks conclude the work in Section 5 together with an outlook on future researches.

2 Micro-Macro decomposition and the limit diffusion equation

In this section, we introduce the micro-macro decomposition of (1.1) for the distribution f [42, 3, 44] which permits to separate the time evolution of the equilibrium part from the time evolution of the perturbation part. This reads

$$f(t,\mathbf{x},\mathbf{v}) = \rho(t,\mathbf{x})M(\mathbf{v}) + g(t,\mathbf{x},\mathbf{v}),\ \ \rho(t,\mathbf{x}) = \langle f\rangle(t,\mathbf{x}) \tag{2.1}$$

with $M(\mathbf{v})$ the Maxwellian equilibrium already introduced, i.e. a Gaussian distribution centered in zero with variance one. The non equilibrium g satisfies by construction for all times

$$\langle g \rangle = 0 \qquad \text{where} \qquad \langle f \rangle = \int_V f(\mathbf{v}) \mathrm{d}\mathbf{v} \tag{2.2}$$

with $V = \mathbb{R}^{d_v}$. In the following, we use the notation $\Pi\phi = \langle \phi \rangle M$ to indicate the orthogonal projection of a function ϕ into the null space $\mathcal{N}$ of the relaxation operator $(\rho(t,\mathbf{x})M(\mathbf{v}) - f(t,\mathbf{x},\mathbf{v}))$. With this notation, the so called microscopic-macroscopic (micro-macro) model reads

$$\begin{cases} \partial_t \rho + \dfrac{1}{\varepsilon} \langle \mathbf{v} \cdot \nabla_{\mathbf{x}} g \rangle = 0, \\ \partial_t g + \dfrac{1}{\varepsilon} \left[\mathbf{v} \cdot \nabla_{\mathbf{x}} \rho M + (I - \Pi)(\mathbf{v} \cdot \nabla_{\mathbf{x}} g) \right] = -\dfrac{1}{\varepsilon^2} g. \end{cases} \tag{2.3}$$

The above model is equivalent to the original one (1.1) and is obtained as follows. We first plug in (1.1) the decomposition (2.1). This gives

$$\partial_t \rho M + \partial_t g + \frac{1}{\varepsilon} \mathbf{v} \cdot \nabla_{\mathbf{x}} \rho M + \frac{1}{\varepsilon} \mathbf{v} \cdot \nabla_{\mathbf{x}} g = -\frac{1}{\varepsilon^2} g. \tag{2.4}$$

Then, we apply $(I - \Pi)$ with I the identity operator to this equation and use $\Pi g = 0$, $\Pi(\partial_t g) = 0$, $\Pi(vM) = 0$, $\Pi(\rho M) = \rho M$ to get the second equation of (2.3). On the other hand, applying Π to equation (2.4) gives the first equation of (2.3). Now, when ε goes to zero, one gets from the second equation of (2.3):

$$g = -\varepsilon(\mathbf{v} \cdot \nabla_{\mathbf{x}} \rho M) + \mathcal{O}(\varepsilon^2). \tag{2.5}$$

Then, the macroscopic equation becomes

$$\partial_t \rho - \langle \mathbf{v} \cdot \nabla_{\mathbf{x}} (\mathbf{v} \cdot \nabla_{\mathbf{x}} \rho M) \rangle = \mathcal{O}(\varepsilon),$$

which gives

$$\partial_t \rho - \Delta_{\mathbf{x}} \rho = \mathcal{O}(\varepsilon).$$

The limit diffusion equation is then obtained by passing to the limit $\varepsilon \to 0$

$$\partial_t \rho - \Delta_{\mathbf{x}} \rho = 0. \tag{2.6}$$

3 A new time diminishing (TDS) asymptotic preserving method

In this section, we present the new numerical method to solve equation (1.1). The main difficulty related to the derivation of a numerical scheme is due to the fact that the scaling parameter ε can range of several order of magnitude both in time and space. Thus, in the situation in which the scaling parameter is small, the problem becomes stiff and in particular this causes the characteristic speeds to grow to infinity. Among the possible solutions, the class of asymptotic preserving method represents certainly a good choice to tackle the method [25, 8, 17, 15], they permit to choose the time step independently of the stiffness of the underlying equation remaining consistent and stable. Here, we propose an alternative which enjoys the same consistency and stability properties but, in

addition, it also permits to reduce the numerical complexity (and then the computational cost) of the problem.

Our first step is presented in the following paragraph and follows the strategy of [15]. Indeed, we propose a reformulation of the micro/macro system (2.3) which permits to surround the stiffness of the transport term. We then propose a particle method to solve the reformulated microscopic equation.

3.1 A time discrete reformulation

The development of a particle-based scheme for equation (1.1) or equivalently for equation (2.3) involves a splitting between the transport and the collision parts. However, while the collision term can be taken implicit, this cannot be done for the transport part. Avoiding the costly inversion of the advection operator, since this transport part is stiff, its exact resolution is faced to the issue of unbounded characteristic speeds. In order to bound the characteristic speeds, we proceed as follows. We first rewrite the micro part of (2.3) by multiplying it by e^{t/ε^2}. This reads

$$\partial_t(e^{t/\varepsilon^2} g) = -\frac{e^{t/\varepsilon^2}}{\varepsilon}\mathcal{F}(\rho, g), \tag{3.1}$$

where $\mathcal{F}(\rho, g)$ is given by

$$\mathcal{F}(\rho, g) = \mathbf{v}\cdot\nabla_{\mathbf{x}}\rho M + \mathbf{v}\cdot\nabla_{\mathbf{x}} g - \langle \mathbf{v}\cdot\nabla_{\mathbf{x}} g\rangle M. \tag{3.2}$$

We denote now by $\Delta t > 0$ a time step and set $t^n = n\Delta t$ with $n \in \mathbb{N}$. By integrating (3.1) on $[t^n, t^{n+1}]$, one gets

$$g(t^{n+1}) = e^{-\Delta t/\varepsilon^2} g(t^n) - \frac{1}{\varepsilon}\int_{t^n}^{t^{n+1}} e^{-(t^{n+1}-\tau)/\varepsilon^2}\mathcal{F}(\rho(\tau), g(\tau))\, d\tau,$$

and then up to an error $\mathcal{O}(\Delta t^2)$

$$g(t^{n+1}) = e^{-\Delta t/\varepsilon^2} g(t^n) - \varepsilon(1 - e^{-\Delta t/\varepsilon^2})\mathcal{F}(\rho(t^n), g(t^n)) + \mathcal{O}(\Delta t^2).$$

Now, one can observe that the above equation can be rewritten as

$$\frac{g(t^{n+1}) - g(t^n)}{\Delta t} = \frac{e^{-\Delta t/\varepsilon^2} - 1}{\Delta t} g(t^n) - \varepsilon\frac{1 - e^{-\Delta t/\varepsilon^2}}{\Delta t}\mathcal{F}(\rho(t^n), g(t^n)) + \mathcal{O}(\Delta t), \tag{3.3}$$

which can be recast, up to an additional error of order $\mathcal{O}(\Delta t)$, as

$$\partial_t g(t^n) = \frac{e^{-\Delta t/\varepsilon^2} - 1}{\Delta t} g(t^n) - \varepsilon\frac{1 - e^{-\Delta t/\varepsilon^2}}{\Delta t}\mathcal{F}(\rho(t^n), g(t^n)) + \mathcal{O}(\Delta t).$$

We now define the first-order in time reformulation of (2.3) as

$$\partial_t \rho + \frac{1}{\varepsilon}\nabla_{\mathbf{x}}\cdot\langle \mathbf{v} g\rangle = 0, \tag{3.4}$$

$$\partial_t g = \frac{e^{-\Delta t/\varepsilon^2} - 1}{\Delta t} g - \varepsilon\frac{1 - e^{-\Delta t/\varepsilon^2}}{\Delta t}\mathcal{F}(\rho, g), \tag{3.5}$$

with $\mathcal{F}(\rho, g)$ given by (3.2). Let us observe that the evolution equation (3.5) for the perturbation g, unlike the second equation of (2.3), does not contain any stiff term. In particular, the characteristic speeds are bounded with respect to ε. Therefore, the approximated model (3.5) appears to be more suitable for a numerical discretization which is constructed following the characteristics equations. Finally, let us remark that this reformulation is consistent with the original model (2.3) in the following sense: when $\Delta t \to 0$, (3.5) converges towards the original microscopic equation of (2.3) for a fixed $\varepsilon > 0$. Let us finally stress that higher order (in time) reformulations of the microscopic model are possible. We do not discuss this possibility here and we refer to [15] for the derivation of a second order approximation of the micro equation of (2.3) which is smooth in ε.

3.2 The Monte-Carlo discretization for the perturbation equation

This subsection is devoted to the derivation of a particle based numerical scheme for equation (3.5). The particle method is based on a time splitting which separates the advection part from the interaction part. It reads

1. **Transport**:
$$\partial_t g + \varepsilon \frac{1 - e^{-\Delta t/\varepsilon^2}}{\Delta t} \mathbf{v} \cdot \nabla_{\mathbf{x}} g = 0, \tag{3.6}$$
2. **Interaction**:
$$\partial_t g = \frac{e^{-\Delta t/\varepsilon^2} - 1}{\Delta t} g - \varepsilon \frac{1 - e^{-\Delta t/\varepsilon^2}}{\Delta t} \left(\mathbf{v} \cdot \nabla_{\mathbf{x}} \rho M - \langle \mathbf{v} \cdot \nabla_{\mathbf{x}} g \rangle M \right). \tag{3.7}$$

The type of scheme we consider is based on stochastic approach and it first consists in replacing the continuous function $g(t, \mathbf{x}, \mathbf{v})$ by a set of $N_p(t)$ particles which occupy random positions $\mathbf{x}_k(t) \in \mathbb{R}^{d_x}$ with random velocities $\mathbf{v}_k(t) \in \mathbb{R}^{d_v}$ and weights ω_k at time t sampled accordingly to $g(t, \mathbf{x}, \mathbf{v})$ as detailed later on. Thus, we consider the following particle approximation of g:

$$g(t, \mathbf{x}, \mathbf{v}) \approx \mu(t, \mathbf{x}, \mathbf{v}) = \sum_{k=1}^{N_p(t)} \omega_k \delta(\mathbf{x} - \mathbf{x}_k(t)) \delta(\mathbf{v} - \mathbf{v}_k(t)),$$

in which δ is the usual Dirac distribution and $\mu(t, \mathbf{x}, \mathbf{v})$ is a so-called empirical distribution. Let us observe that the above choice corresponds to constant weights ω_k while the number of particles in the domain may change with time. An alternative particle approach may consist in taking time-dependent weights $\omega_k(t)$ while maintaining constant their number [44]. Starting from the empirical distribution, one needs to reconstruct the particle densities in phase space during the time evolution of the solution. Restricting ourselves to the one dimensional case for simplicity, these densities are obtained by introducing a mesh in the phase space and computing the histogram on this mesh in the cell centers x_i and v_ℓ with corresponding mesh sizes Δx and Δv:

$$g(t, x_i, v_\ell) = \int_{x_i - \Delta x/2}^{x_i + \Delta x/2} \int_{v_\ell - \Delta v/2}^{v_\ell + \Delta v/2} 1 \cdot d\mu(t, x, v). \tag{3.8}$$

In practice, we use the following formulae

$$g(t, x_i, v_\ell) = \frac{1}{\Delta x \Delta v} \sum_{\substack{k=1,\dots,N_p(t) \\ (x_k(t), v_k(t)) \in C_{i,\ell}}} \omega_k,$$

where $C_{i,\ell} = [x_i - \Delta x/2, x_i + \Delta x/2] \times [v_\ell - \Delta v/2, v_\ell + \Delta v/2]$. The extension to the multidimensional case of such reconstruction is straightforward.

It remains to define the weights ω_k. This is done as follows. We first define the mass m_p of an individual particle representing a portion of the distribution $f(t = 0, \mathbf{x}, \mathbf{v})$ as

$$m_p = \frac{1}{N_p(t=0)} \int_{\mathbb{R}^{d_x}} \int_{\mathbb{R}^{d_v}} f(t = 0, \mathbf{x}, \mathbf{v}) d\mathbf{v} d\mathbf{x}. \tag{3.9}$$

Successively, we assign to a particle a positive or negative weight. This is a consequence of the fact that the perturbation g is not positive everywhere and this contrasts with the usual particle methods which are applied on the full distribution function f (in this case particles have only positive weights since f is positive by definition). Thus, the weights ω_k are chosen either positive $\omega_k = m_p$ if k belongs to the subset of the $N_p(t)$ particles used to represent the positive part of the microscopic function g, i.e. $k \in \mathcal{N}^+ \subseteq [\![1, N_p]\!]$, or negative in the opposite case $\omega_k = -m_p$ if $k \in \mathcal{N}^- \subseteq [\![1, N_p]\!]$: the subset of the particles used for representing the negative part of g. For consistency we have $\mathcal{N}^+ \cap \mathcal{N}^- = \emptyset$, while the accuracy of the method is related to the choice of the mass m_p: smaller is the mass m_p, larger is the accuracy of the method.

At time $t = 0$, the number of particles is given by

$$N^{0,\pm} = \pm \frac{1}{m_p} \int_{\mathbb{R}^{d_x}} \int_{\mathbb{R}^{d_v}} g^{\pm}(t = 0, \mathbf{x}, \mathbf{v}) d\mathbf{v} d\mathbf{x},$$

where the positive (respectively the negative) part of g is

$$g^{\pm} = (g \pm |g|)/2. \tag{3.10}$$

Since the integrals of $g^{\pm}$ have no reason to be integers we associate to any real number a the integer

$$\lfloor a \rfloor \qquad \text{with probability} \qquad 1 - a + \lfloor a \rfloor$$

and the integer

$$\lfloor a \rfloor + 1 \qquad \text{with probability} \qquad a - \lfloor a \rfloor$$

where $\lfloor a \rfloor$ is the integer part of a. All the real expressions defining integers have to be interpreted with the above meaning.

In the sequel, we denote by $C_{i,\ell} \subset \mathbb{R}^{d_x} \times \mathbb{R}^{d_v}$ the cell centered around the point $(\mathbf{x}_i, \mathbf{v}_\ell)$ and by $N_{i,\ell}^{n,+}$ (resp. $N_{i,\ell}^{n,-}$) the number of positive (resp. negative) particles in $C_{i,\ell}$ at time t^n. Initially, we use in the 1-dimensional framework the following definition

$$N_{i,\ell}^{0,\pm} = \pm \frac{1}{m_p} \int_{x_i - \Delta x/2}^{x_i + \Delta x/2} \int_{v_\ell - \Delta v/2}^{v_\ell + \Delta v/2} g^{\pm}(t = 0, x, v) dv dx,$$

and approximate it by $N_{i,\ell}^{0,\pm} = \pm \frac{\Delta x \Delta v}{m_p} g^{\pm}(t = 0, x_i, v_\ell)$. The extension of this definition to the multidimensional case is straightforward.

For the positive particles in $C_{i,\ell}$, the sampling is then defined as follows: for all $k = 1, \ldots, N_{i,\ell}^{0,+}$, the velocities $\mathbf{v}_k^0$ are assigned to $\mathbf{v}_\ell$, the positions $\mathbf{x}_k^0$ are uniformly distributed in the cell $C_i = \cup_l C_{i,\ell}$, and the weights $\omega_k = m_p$. The same strategy is used for negative particles, expects the weights that are defined as $\omega_k = -m_p$.

Moreover, we introduce $N_i^{n,\pm} = \sum_\ell N_{i,\ell}^{n,\pm}$ and $N_i^n = N_i^{n,+} + N_i^{n,-}$ the total number of particles in C_i at time t^n, $n \geq 0$, and finally $N^n = \sum_i N_i^n$.

Thanks to the above described setting and notations, we are now ready to detail our algorithm step by step. Thus, we start with an initial sampling of the $N_p(t=0)$ particles $(\mathbf{x}_k^0, \mathbf{v}_k^0)$ which approximates the initial micro unknown $g(t=0,\mathbf{x},\mathbf{v})$, as described previously. Then at each time step Δt, we follow the splitting procedure presented at the beginning of this subsection.

1. We solve the transport part by shifting particles

$$\mathbf{x}_k^{n+1} = \mathbf{x}_k^n + \Delta t \varepsilon (1 - e^{-\Delta t/\varepsilon^2}) \mathbf{v}_k^n. \tag{3.11}$$

   The velocities of the particles do not change in this step. This defines an intermediate empirical distribution from which an intermediate particle density $\tilde{g}^n(\mathbf{x},\mathbf{v})$ can be recovered by the formulae

$$\tilde{g}^n(\mathbf{x},\mathbf{v}) \simeq \tilde{\mu}^n(\mathbf{x},\mathbf{v}) = \sum_{k=1}^{N^n} \omega_k \delta(\mathbf{x} - \mathbf{x}_k^{n+1}) \delta(\mathbf{v} - \mathbf{v}_k^n) \tag{3.12}$$

   and then used for solving the next step. In particular, this gives the values $\tilde{g}^n(\mathbf{x}_i, \mathbf{v}_\ell)$ in the cell $C_{i,\ell}$. In the 1-dimensional case, the formulae writes

$$\tilde{g}^n(x_i, v_\ell) = \frac{1}{\Delta x \Delta v} \sum_{\substack{k=1,\dots,N_p^n \\ (x_k^{n+1}, v_k^{n+1}) \in C_{i,\ell}}} \omega_k \tag{3.13}$$

   and is easily extended in the multidimensional case.

   Since particles have moved in this transport part, we denote by $\tilde{N}_i^{n,+}$ (resp. $\tilde{N}_i^{n,+}$) the number of positive (resp. negative) particles in C_i after the transport step, and we define $\tilde{N}_i^n = \tilde{N}_i^{n,+} + \tilde{N}_i^{n,-}$.

2. We solve the interaction part by reporting $\partial_t g \sim \frac{g^{n+1} - g^n}{\Delta t}$ into (3.7):

$$g^{n+1} = e^{-\Delta t/\varepsilon^2} \tilde{g}^n + (1 - e^{-\Delta t/\varepsilon^2}) \varepsilon \big[-\mathbf{v} \cdot \nabla_{\mathbf{x}} \rho^n M + \nabla_{\mathbf{x}} \cdot \langle \mathbf{v} \tilde{g} \rangle^n M \big], \tag{3.14}$$

   where the function $\tilde{g}^n$ is defined by (3.13). In the following we give details about how this step is solved with stochastic particles.

   One can observe that g^{n+1} in (3.14) is written as a linear combination of $\tilde{g}^n$ and a given analytic function in $\mathbf{v}$. At the Monte Carlo level, the above formulae can be interpreted in the following way:

   - with probability $e^{-\Delta t/\varepsilon^2}$, the distribution g^{n+1} does not change,
   - with probability $(1 - e^{-\Delta t/\varepsilon^2})$, the distribution g^{n+1} is replaced by a new distribution given by $\varepsilon \big[-\mathbf{v} \cdot \nabla_{\mathbf{x}} \rho^n M + \nabla_{\mathbf{x}} \cdot \langle \mathbf{v} \tilde{g} \rangle^n M \big]$.

   In practice, this means that

   - a fraction $e^{-\Delta t/\varepsilon^2}$ of particles is kept with unchanged velocity and position. More precisely, in each cell C_i we keep $e^{-\Delta t/\varepsilon^2} \tilde{N}_i^n$ particles and discard the rest uniformly.

- We define the function $\mathcal{P}^{n,\pm}(\mathbf{x},\mathbf{v}) = \varepsilon\big[-\mathbf{v}\cdot\nabla_{\mathbf{x}}\rho^n M + \nabla_{\mathbf{x}}\cdot\langle\mathbf{v}\tilde{g}\rangle^n M\big]^{\pm}$ where positive and negative parts are defined like in (3.10). One samples a corresponding number $M_i^{n,\pm}$ of particles with weights $\pm m_p$ from $\mathcal{P}^{n,\pm}(\mathbf{x}_i,\mathbf{v})$ in each spatial cell C_i uniformly in space representing the distribution at the Monte Carlo level. For this sampling, we create $M_{i,\ell}^{n,\pm}$ particles in the cell $C_{i,\ell}$. In the 1-dimensional case, this number

$$M_{i,\ell}^{n,\pm} = \frac{1}{m_p}\int_{x_i-\Delta x/2}^{x_i+\Delta x/2}\int_{v_\ell-\Delta v/2}^{v_\ell+\Delta v/2} \pm\mathcal{P}^{n,\pm}(x,v)dvdx,$$

is approximated by $M_{i,\ell}^{n,\pm} = \pm\frac{\Delta x\Delta v}{m_p}\mathcal{P}^{n,\pm}(x_i,v_\ell)$. This formulae is directly extended in the multidimensional case. To these particles in $C_{i,\ell}$, we assigned velocities $\mathbf{v}_k^n = \mathbf{v}_\ell$, positions $\mathbf{x}_k^n$ that are uniformly distributed in the cell $C_i = \cup_\ell C_{i,\ell}$, and weights $\omega_k = \pm m_p$.

However, only a fraction $(1-e^{-\Delta t/\varepsilon^2})$ of $M_i^n = \sum_\ell M_{i,\ell}^{n,+} + \sum_\ell M_{i,\ell}^{n,-}$ is kept for the next time step. When $\varepsilon\sim 1$, the number of particles may increase with this procedure, that is why we consider a maximal number of particles and do not create new ones if this threshold is reached. On the contrary when ε is small, we create few particles. Thanks to the discarding procedure, the total number of particles decreases with time, so that our strategy is Time-Diminishing.

Let us notice that in practice we directly sample the $M_i^{n,\pm}$ particles from the distribution $(1-e^{-\Delta t/\varepsilon^2})\mathcal{P}^{n,\pm}(\mathbf{x}_i,\mathbf{v})$, instead of sampling from $\mathcal{P}^{n,\pm}(\mathbf{x}_i,\mathbf{v})$. In this way, we do not need to discard the proportion $e^{-\Delta t/\varepsilon^2}M_i^{n,\pm}$ of particles. This highly simplifies the above approach and automatically allows to diminish the number of used particles as $\varepsilon\to 0$. Finally, for the next time step the number of particles becomes $N_i^{n+1} = e^{-\Delta t/\varepsilon^2}\tilde{N}_i^n + M_i^n$ and the above procedure can be iterated to advance in time.

The method described deserves some remarks. First, it permits to overcome the stiffness related to the characteristic speeds allowing for time steps independent of the scaling parameter ε. Second, it automatically diminishes the computational complexity as $\varepsilon\to 0$: the number of particles diminishes linearly with the scaling parameter. This is opposite to standard Monte Carlo or more general particle approaches for kinetic equations, where the computational complexity remains unchanged with ε. This highlights the TDS property of our strategy.

3.3 A finite volume method for the macroscopic equation

In this subsection, we focus on the space-time discretization of the macroscopic equation (3.4). One natural choice would be the following time discretization (see [42])

$$\frac{\rho^{n+1}-\rho^n}{\Delta t} + \frac{1}{\varepsilon}\nabla_{\mathbf{x}}\cdot\langle\mathbf{v}g^{n+1}\rangle = 0, \tag{3.15}$$

where the value g^{n+1} would be recovered from the Monte Carlo solution of equation (3.5). This would permit to overcome the stiffness in (3.15) and would lead to a numerical scheme which is stable for all time steps and is consistent with the limit diffusion equation scheme. However, due to the stochastic approximation, g^{n+1} may suffer from noise which will be passed on the macroscopic unknown ρ^{n+1}. This statistical noise, inherent to particle methods, will be amplified by the factor

$1/\varepsilon$ so that from one side it would be more difficult to stabilize a finite volume method and from the other side the asymptotic behavior could be lost. To overcome this drawback, we then propose to separate in the expression of g^{n+1} given by (3.14) the macroscopic term containing ρ^n which gives rise to the limit diffusion equation (2.6) from the microscopic ones.

Thus, starting from (3.14), let us first compute $\langle \mathbf{v}\cdot\nabla_{\mathbf{x}} g^{n+1}\rangle$:

$$\begin{aligned}\langle \mathbf{v}\cdot\nabla_{\mathbf{x}} g^{n+1}\rangle = e^{-\Delta t/\varepsilon^2}\langle \mathbf{v}\cdot\nabla_{\mathbf{x}}\tilde{g}^n\rangle - \varepsilon(1-e^{-\Delta t/\varepsilon^2})\\ \left(\langle \mathbf{v}\cdot\nabla_{\mathbf{x}}\left(\mathbf{v}\cdot\nabla_{\mathbf{x}}\rho^n M\right)\rangle - \langle \mathbf{v}\cdot\nabla_{\mathbf{x}}\left(\langle \mathbf{v}\cdot\nabla_{\mathbf{x}}\tilde{g}\rangle^n M\right)\rangle\right).\end{aligned}$$

Since $\langle \mathbf{v}\cdot\nabla_{\mathbf{x}}\tilde{g}\rangle^n$ does not depend on $\mathbf{v}$ and $\langle \mathbf{v}M\rangle = \mathbf{0}$, we get

$$\langle \mathbf{v}\cdot\nabla_{\mathbf{x}} g^{n+1}\rangle = e^{-\Delta t/\varepsilon^2}\langle \mathbf{v}\cdot\nabla_{\mathbf{x}}\tilde{g}^n\rangle - \varepsilon(1-e^{-\Delta t/\varepsilon^2})\langle \mathbf{v}\cdot\nabla_{\mathbf{x}}\left(\mathbf{v}\cdot\nabla_{\mathbf{x}}\rho^n M\right)\rangle$$

and finally

$$\langle \mathbf{v}\cdot\nabla_{\mathbf{x}} g^{n+1}\rangle = e^{-\Delta t/\varepsilon^2}\langle \mathbf{v}\cdot\nabla_{\mathbf{x}}\tilde{g}^n\rangle - \varepsilon(1-e^{-\Delta t/\varepsilon^2})\Delta_{\mathbf{x}}\rho^n. \tag{3.16}$$

Plugging expression (3.16) into the macro equation (3.15), we get

$$\frac{\rho^{n+1}-\rho^n}{\Delta t} + \frac{1}{\varepsilon}e^{-\Delta t/\varepsilon^2}\langle \mathbf{v}\cdot\nabla_{\mathbf{x}}\tilde{g}^n\rangle - (1-e^{-\Delta t/\varepsilon^2})\Delta_{\mathbf{x}}\rho^n = 0.$$

We now observe that the above time discretization permits to remove the stiffness that appeared in (3.15) when $\varepsilon\to 0$, but the diffusion turns out to be explicit. Therefore, this requires a parabolic CFL condition of type $\Delta t \le C\Delta x^2$. To avoid such restrictive condition, an implicit treatment of the asymptotic heat equation may be adopted so that the time discretization of the macro unknown becomes

$$\frac{\rho^{n+1}-\rho^n}{\Delta t} + \frac{1}{\varepsilon}e^{-\Delta t/\varepsilon^2}\nabla_{\mathbf{x}}\cdot\langle \mathbf{v}\tilde{g}^n\rangle - (1-e^{-\Delta t/\varepsilon^2})\Delta_{\mathbf{x}}\rho^{n+1} = 0. \tag{3.17}$$

Note that this choice allows larger time steps, and that equation (3.5) may be modified accordingly in this case:

$$g^{n+1} = e^{-\Delta t/\varepsilon^2}\tilde{g}^n + (1-e^{-\Delta t/\varepsilon^2})\varepsilon\big[-\mathbf{v}\cdot\nabla_{\mathbf{x}}\rho^{n+1}M + \nabla_{\mathbf{x}}\cdot\langle \mathbf{v}\tilde{g}\rangle^n M\big]. \tag{3.18}$$

Luckily, equations (3.17) and (3.18) can still be solved separately by first solving implicitly equation (3.17) which needs only the knowledge of $\tilde{g}^n$ which is obtained by the advection step of the time splitting algorithm described in (3.2). Successively one can solve (3.18) with the value ρ^{n+1} found in (3.17).

We finally discuss the space discretization. We choose for (3.17) a simple centered finite difference approximation of $\nabla_{\mathbf{x}}\cdot\langle \mathbf{v}\tilde{g}^n\rangle$. Concerning the space approximation of the Laplacian term, we use an ADI (Alternating Direction Implicit) method (see [47]) to avoid the inversion of large matrices in the multidimensional cases, still avoiding parabolic CFL condition. We give details in the two dimensional case $d_x = 2$ in space ($\mathbf{x} = (x,y)$). In this case, the method reduces to the following splitting, starting from ρ^n.

1. We solve over a time step Δt the equation $\partial_t\rho + \frac{1}{2\varepsilon}e^{-\Delta t/\varepsilon^2}\langle \mathbf{v}\cdot\nabla_{\mathbf{x}}\tilde{g}^n\rangle - (1-e^{-\Delta t/\varepsilon^2})\partial_{xx}\rho = 0$, using a Crank-Nicolson time discretization to get $\rho^\star$.

2. Starting from $\rho^\star$, we solve over a time step Δt the equation $\partial_t \rho + \frac{1}{2\varepsilon} e^{-\Delta t/\varepsilon^2} \langle \mathbf{v} \cdot \nabla_{\mathbf{x}} \tilde{g}^n \rangle - (1 - e^{-\Delta t/\varepsilon^2}) \partial_{yy} \rho = 0$, using a Crank-Nicolson time discretization to get ρ^{n+1}.

Given $x_i = x_{min} + (i-1)\Delta x$, $y_j = y_{min} + (j-1)\Delta y$, a cartesian mesh of size $(\Delta x, \Delta y)$ with N_x and N_y points, we define $\rho^n_{i,j}$ an approximation of $\rho(t^n, x_i, y_j)$, and $\langle \mathbf{v}\tilde{g}^n \rangle_{i,j}$ an approximation of the first moment $\langle \mathbf{v}\tilde{g}(t^n, x_i, y_j) \rangle$, with $\mathbf{v} = (v_x, v_y)$. Then, the corresponding time-space discretization is the following.

1. For each fixed j such that $1 \leq j \leq N_y$, solve the one-dimensional system of size N_x

$$
\begin{aligned}
-\frac{\Delta t}{2\Delta x^2}(1 - e^{-\Delta t/\varepsilon^2})\rho^\star_{i+1,j} + \left(1 + \frac{\Delta t}{\Delta x^2}(1 - e^{-\Delta t/\varepsilon^2})\right)\rho^\star_{i,j} - \frac{\Delta t}{2\Delta x^2}(1 - e^{-\Delta t/\varepsilon^2})\rho^\star_{i-1,j} \\
= \rho^n_{i,j} - \frac{\Delta t}{2\varepsilon} e^{-\Delta t/\varepsilon^2} \left(\frac{\langle v_x \tilde{g}^n \rangle_{i+1,j} - \langle v_x \tilde{g}^n \rangle_{i-1,j}}{2\Delta x} + \frac{\langle v_y \tilde{g}^n \rangle_{i,j+1} - \langle v_y \tilde{g}^n \rangle_{i,j-1}}{2\Delta y} \right) \\
+ \frac{\Delta t}{2}(1 - e^{-\Delta t/\varepsilon^2}) \frac{\rho^n_{i+1,j} - 2\rho^n_{i,j} + \rho^n_{i-1,j}}{\Delta x^2},
\end{aligned}
$$

   which furnishes the intermediate values $\rho^\star_{1 \leq i \leq N_x, j}$.

2. For each fixed i such that $1 \leq i \leq N_x$, solve the one-dimensional system of size N_y

$$
\begin{aligned}
-\frac{\Delta t}{2\Delta y^2}(1 - e^{-\Delta t/\varepsilon^2})\rho^{n+1}_{i,j+1} + \left(1 + \frac{\Delta t}{\Delta y^2}(1 - e^{-\Delta t/\varepsilon^2})\right)\rho^{n+1}_{i,j} - \frac{\Delta t}{2\Delta y^2}(1 - e^{-\Delta t/\varepsilon^2})\rho^{n+1}_{i,j-1} \\
= \rho^\star_{i,j} - \frac{\Delta t}{2\varepsilon} e^{-\Delta t/\varepsilon^2} \left(\frac{\langle v_x \tilde{g}^n \rangle_{i+1,j} - \langle v_x \tilde{g}^n \rangle_{i-1,j}}{2\Delta x} + \frac{\langle v_y \tilde{g}^n \rangle_{i,j+1} - \langle v_y \tilde{g}^n \rangle_{i,j-1}}{2\Delta y} \right) \\
+ \frac{\Delta t}{2}(1 - e^{-\Delta t/\varepsilon^2}) \frac{\rho^\star_{i,j+1} - 2\rho^\star_{ij} + \rho^\star_{i,j-1}}{\Delta y^2},
\end{aligned}
$$

   which gives the value of the density at time $n+1$: $\rho^{n+1}_{i,1 \leq j \leq N_y}$.

It is known that the ADI method is conditionally stable in the three dimensional case, even if some uniformly stable extensions have been derived [49]. We conclude this part by stressing that the proposed method is stable independently of the choice of the time step, thanks to the two following ingredients: (i) the approximation of the microscopic part is unconditionally stable due to the reformulation and the use of a particles method; (ii) the approximation of the macroscopic part is free from the CFL parabolic condition due to the use of a implicit or semi-implicit method for the diffusion term.

4 Numerical results

We present in this section several numerical results with the scope of understanding the behaviors and the characteristics of the proposed method. The two first subsections aim at validating the Hybrid Micro-Macro Monte Carlo scheme described in the previous section. They concern four dimensional phase space experiments ($d_x = d_v = 2$). In these cases, our method is compared to other known approaches: namely a micro-macro grid method (see [17, 42]) considered as a reference, a full particle scheme performed on the original distribution function f, or a finite difference method

for the asymptotic diffusion equation. Diagnostics on macroscopic variables as well as $\mathbf{v}$-dependent quantities are presented. Numerical cost reduction measures - linked to the time-diminishing (TDS) property - are discussed, in order to point out the efficiency of our method. After these validating tests, we highlight other advantages of our method, namely the possibility of considering space-dependent scaling parameter ε and the performances in higher dimension. To that aim, in the third subsection, we present a slightly different model, in which a space-dependent collisional frequency is considered. We show how the Hybrid Micro-Macro Monte Carlo method is automatically able to adapt the number of particles to the collision frequency. Finally, we propose a full 3D in space and 3D in velocity test case to show the ability of our approach to deal with problems of physical relevance.

4.1 Two-dimensional test cases with constant scaling parameter and equilibrium initial condition

This subsection is devoted to 2D-2D numerical results in the constant ε case and with an equilibrium initial condition given by

$$f(t=0,\mathbf{x},\mathbf{v}) = \rho(t=0,\mathbf{x})M(\mathbf{v}),\ \mathbf{x}\in[0,4\pi]^2,\ \mathbf{v}\in\mathbb{R}^2 \tag{4.19}$$

with $\rho(t=0,\mathbf{x}) = 1+\frac{1}{2}\cos\left(\frac{x}{2}\right)\cos\left(\frac{y}{2}\right)$, $M(\mathbf{v}) = \frac{1}{2\pi}\exp\left(-\frac{|\mathbf{v}|^2}{2}\right)$, so that $g(t=0,\mathbf{x},\mathbf{v})=0$. Periodic boundary conditions are imposed in space. The aim is to compare our Hybrid Micro-Macro Monte Carlo approach, referred to as "MM-MC" in the sequel, with other methods. Namely, we compare the MM-MC with the following methods.

- A micro-macro grid approach (referred to as "MM-G"). Considering the model described by equations (3.4)-(3.5), g is discretized on a grid in space and in velocity. This method has been shown to be uniformly stable independently of the scaling parameter ε and asymptotically consistent with the diffusion equation (see [42] for details). When the meshes are refined enough, we will take the solution provided by MM-G as a reference solution for comparisons.

- A full particle method (referred to as "Full MC"). We use a classical particle method directly on model (1.1). We refer to [6] for details about this approach. At the limit $\varepsilon\to 0$, this method suffers from a severe constraint on the time step: it has to be of order ε^2. For this reason, we shall only use it in regimes where ε is of order 1.

- A finite difference discretization for the limit equation (referred to as "Limit"). When the scaling parameter ε is small, we use finite differences in space and an ADI Crank-Nicolson scheme in time for discretizing the limit diffusion equation, as explained in Subsection 3.3.

We recall that the solution of a refined MM-G will be taken as a reference solution, whereas the full particle method represents the solutions that can be obtained by a standard Monte Carlo approach. In this part, we aim at showing that our method performs better than a standard Monte Carlo approach in terms of computational cost and reduction of the fluctuations, and than deterministic approaches in terms of computational cost.

Figure	Scheme	N_x, N_y	m_p	N_{v_x}, N_{v_y}	Δt	ε	T
1f	Limit	128			0.1		2
1b, 2a	MM-MC	128	10^{-6}		0.1	0.0001	2
1c, 2b	MM-MC	128	10^{-6}		0.1	0.1	2
1d, 2c	MM-G	128		10	0.01	0.0001	2
1e, 2d	MM-G	128		10	0.0005	0.1	2

Table 1: Numerical parameters for the MM-MC, MM-G and the finite difference method for the limit diffusion equation.

Limit and intermediate regimes. We start by analyzing the MM-MC method in the limit and intermediate regimes. To that aim, we consider two different values of the scaling parameter ε: 0.1 and 0.0001. In Figure 1, we report the density $\rho(T, \mathbf{x})$ at the final time of the simulation fixed at $T = 2$ for different schemes, while $\rho(0, \mathbf{x})$ is reported in Figure 1a. In particular, we compare the solutions given by our MM-MC approach with the MM-G approach. Table 1 reports the numerical parameters chosen for the above described simulations.

In Figure 1b the MM-MC is reported for $\varepsilon = 0.0001$ while in Figure 1c for $\varepsilon = 0.1$. In Figure 1d and 1e the results obtained with the MM-G approach are shown. For these two values of the scaling parameter, the solutions are both very close to the limit solution which is reported in Figure 1f. We can claim that the correct asymptotic behavior is observed by both the MM-MC and the MM-G methods especially for $\varepsilon = 0.0001$.

The deviation from equilibrium for the different values of the scaling parameters can be measured by performing a diagnostic on the non equilibrium part of the momentum variable $\langle v_x g \rangle(t, \mathbf{x})$. To that aim, in Figure 2, we report the momentum at the final time of the simulation $\langle v_x g \rangle(T = 2, \mathbf{x})$. This quantity is fixed to zero at the beginning, in fact equilibrium initial data are chosen, and it should remain zero in the limit $\varepsilon \to 0$. For $\varepsilon = 0.0001$ (respectively $\varepsilon = 0.1$), results given by the MM-MC approach are presented in Figure 2a (respectively 2b) while the results given by the MM-G approach are presented in Figure 2c (respectively 2d). We observe from the simulations that the component of the momentum given by the perturbation g diminishes as ε goes to zero, as theoretically expected. So we can claim that both approaches share a good asymptotic behavior, i.e. are asymptotically consistent. Moreover, we can observe that the MM-MC method produces some statistical oscillations which automatically diminish when the scaling parameter decreases, since the number of particles used in the simulation is proportional to the perturbation g (let us remark that when $\varepsilon = 10^{-6}$ there is almost no particles at $T = 2$). We emphasize that this noise can also be reduced by imposing a higher number of particles, or equivalently a smaller typical weight m_p for each particle. We finally compare the results by considering the slice $y = 0$. Figure 3a shows the slice density $\rho(T = 2, x, y = 0)$ while in Figure 3b the slice momentum $\langle v_x g \rangle(T = 2, x, y = 0)$ for $\varepsilon = 0.1$ and $\varepsilon = 0.0001$ is shown. We can finally claim that for these test cases, the MM-MC method is able to reproduce the correct solution identified by the reference furnished by the MM-G scheme.

Concerning the choice of the time step, the MM-MC method is stable independently of the time step Δt. On the contrary, the MM-G scheme, as other grid based schemes, suffers from a constraint on Δt related to the speed of the particles.

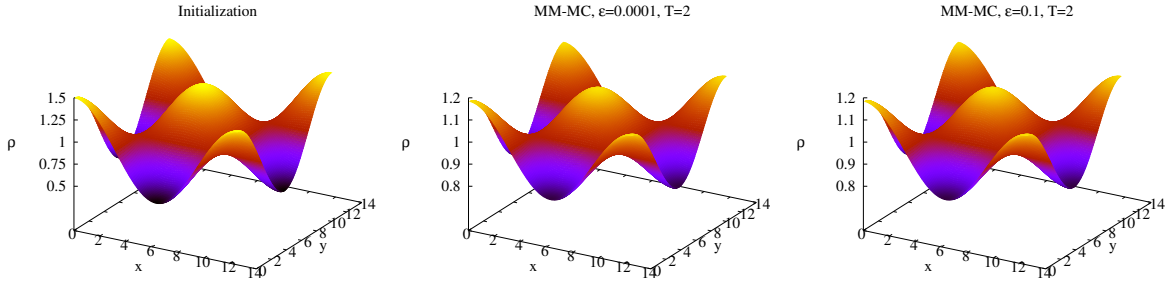

(a) Initialization, $T = 0$ (b) MM-MC method, $T = 2$, $\varepsilon = 0.0001$ (c) MM-MC method, $T = 2$, $\varepsilon = 0.1$

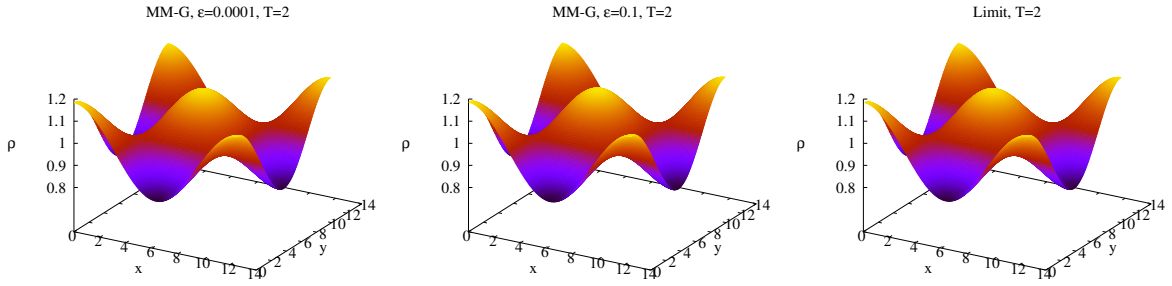

(d) MM-G method, $T = 2$, $\varepsilon = 0.0001$ (e) MM-G method, $T = 2$, $\varepsilon = 0.1$ (f) Limit, $T = 2$

Figure 1: The density profile ρ is shown for the MM-MC, the MM-G methods and for the limit diffusion equation in the limit and the intermediate regimes.

Kinetic regime. In this part, we are interested in the numerical results when ε is of order 1, we refer to this regime as the kinetic regime. The initialization is the same as for the previous case (see (4.19) and Figure 1a for the density profile at $T = 0$). Table 2 reports the numerical parameters chosen for the following simulations.

Figure 4 shows the density profile at time $T = 2$, whereas the momentum $\langle v_x f \rangle$ is reported in Figure 5. For $\varepsilon = 0.5$ (respectively $\varepsilon = 1$), we report the density obtained when a full Monte Carlo method (referred to as "Full MC") is employed to compute the solution. In Figure 4a (respectively 4d) these density profiles are shown for the two different values of ε. As well known, a full Monte Carlo method suffers from large numerical noise especially when non stationary problems are solved. This fact is made clear by the simulation reported in which 10^8 particles are used in the simulations. This corresponds to a particle weight of order 10^{-6}. On the contrary with respect to the full particle scheme, the MM-MC produces solutions with much less oscillations as shown in Figure 4b for $\varepsilon = 0.5$ (respectively 4e for $\varepsilon = 1$) with the same typical weight m_p. In both cases, the results of the MM-MC method are very close to the ones of the MM-G reference method shown in Figure 4c for $\varepsilon = 0.5$ (respectively 4f for $\varepsilon = 1$).

Concerning the momentum, we show the quantity $\langle v_x f \rangle$ given by the Full MC method in Figure 5a for $\varepsilon = 0.5$ and in Figure 5d for $\varepsilon = 1$. The numerical noise strongly affects this quantity. For

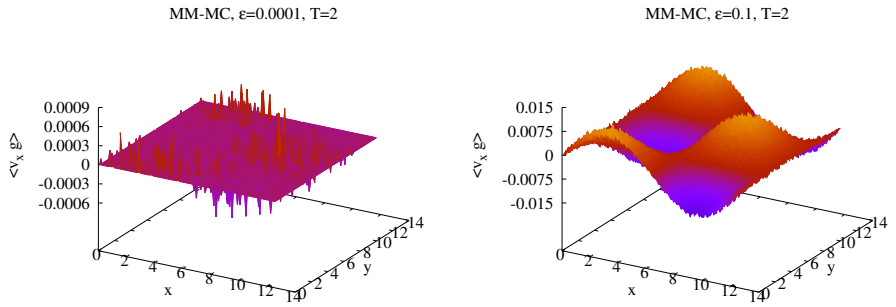

(a) MM-MC method, $T = 2$, $\varepsilon = 0.0001$ (b) MM-MC method, $T = 2$, $\varepsilon = 0.1$

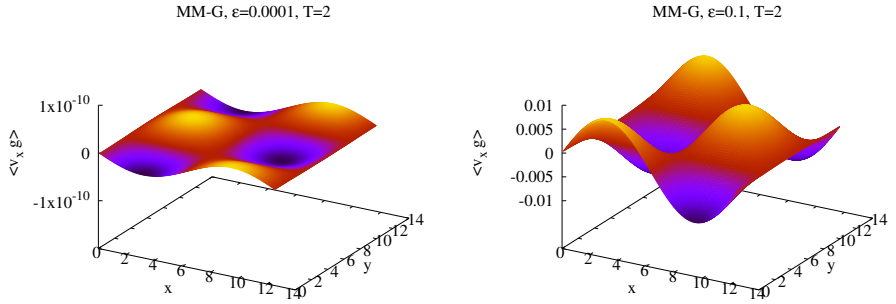

(c) MM-G method, $T = 2$, $\varepsilon = 0.0001$ (d) MM-G method, $T = 2$, $\varepsilon = 0.1$

Figure 2: The component of the momentum given by the perturbation g, $\langle v_x g \rangle$, is shown for the MM-MC and the MM-G methods and for different values of the scaling parameter ε in the limit and intermediate regimes.

the MM-MC method, the corresponding quantity $\langle v_x g \rangle$ is presented in Figure 5b and in Figure 5e for the two different values of the scaling parameters while the results for the MM-G approach are presented in Figure 5c and in Figure 5f. As for the case of the limit and intermediate regimes, we report the density and the momentum profiles for a slice in $y = 0$. The density $\rho(T = 2, x, y = 0)$ is shown in Figure 6a, while the momentum $\langle v_x f \rangle(T = 2, x, y = 0)$ is shown in Figure 6b for the case $\varepsilon = 1$.

Time-diminishing property. In this part, we are interested in measuring the computational cost of the method as well as measuring the so-called time-diminishing (TDS) property of our MM-MC method. This latter means the capacity of the scheme to diminish its computational complexity as the limit diffusion equation is approached. We highlight these properties through the evolution in time of the total number of particles $N_p(t)$. In Figure 7a, we present the results obtained in the 2D-2D case where the initial condition is given by (4.19) and where ε takes the values 1, 0.5, 0.2 and 0.1. As the perturbation g is initially zero, the number of particles at the beginning increases due to the fact that the transport phase induces departure from equilibrium. Then, due to collisions, the system approaches the equilibrium again and the number of particles decreases. The smaller is ε, the smaller is g and the smaller is the number of particles we need to

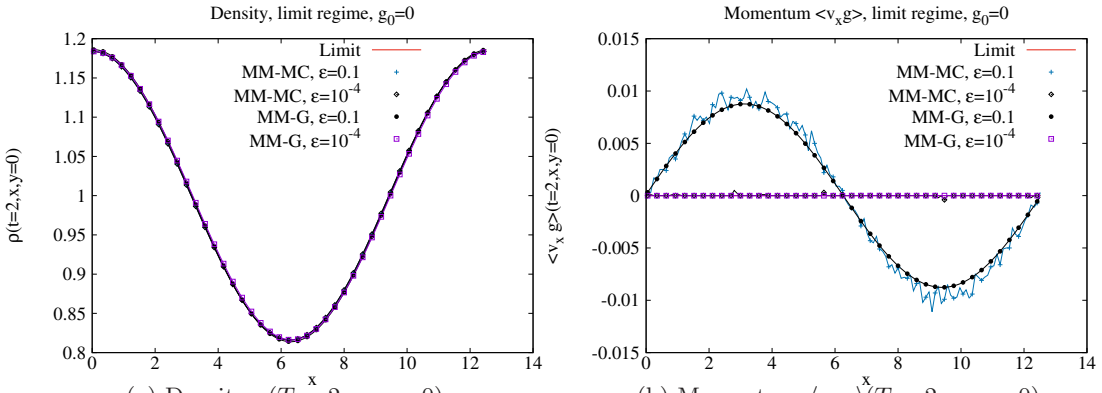

(a) Density $\rho(T=2,x,y=0)$ (b) Momentum $\langle v_x g\rangle(T=2,x,y=0)$

Figure 3: Slices of the density $\rho(T=2,x,y=0)$ and of the momentum $\langle v_x g\rangle(T=2,x,y=0)$ in the limit and intermediate regimes. Comparisons between the MM-MC, the MM-G and the limit diffusion equation.

Figure	Scheme	N_x, N_y	Typical weight	N_{v_x}, N_{v_y}	Δt	ε	T
4a, 5a	Full MC	128	10^{-6}		0.1	0.5	2
4d, 5d	Full MC	128	10^{-6}		0.1	1	2
4b, 5b	MM-MC	128	10^{-6}		0.1	0.5	2
4e, 5e	MM-MC	128	10^{-6}		0.1	1	2
4c, 5c	MM-G	128		10	0.001	0.5	2
4f, 5f	MM-G	128		10	0.005	1	2

Table 2: Numerical parameters for the Full MC, the MM-MC and the MM-G methods for the kinetic regime.

represent this component of the solution. This behaviour is confirmed by Figure 7b, where results are given for $\varepsilon = 0.01$, $\varepsilon = 0.001$ and $\varepsilon = 0.0001$.

4.2 Two-dimensional test cases with non-equilibrium initial condition and constant scaling parameter

In this part, we consider the following non-equilibrium initial data for the distribution function f

$$f(t=0,\mathbf{x},\mathbf{v}) = \frac{1}{4\pi}\left(\exp\left(-\frac{|\mathbf{v}-2|^2}{2}\right)+\exp\left(-\frac{|\mathbf{v}+2|^2}{2}\right)\right)\rho(t=0,\mathbf{x}),\ \ \mathbf{x}\in[0,4\pi]^2,\ \ \mathbf{v}\in\mathbb{R}^2, \tag{4.20}$$

with $\rho(t=0,\mathbf{x}) = 1+\frac{1}{2}\cos\left(\frac{x}{2}\right)\cos\left(\frac{y}{2}\right)$. The tests presented use the parameters detailed in Table 3. In this part, we look at quantities depending only on the velocity space: i.e. v_x and v_y. More precisely, we compute $\int f(t,\mathbf{x},\mathbf{v})d\mathbf{x}$ and $\int g(t,\mathbf{x},\mathbf{v})d\mathbf{x}$ from the MM-MC method and we compare the results from the MM-G one. We present in Figures 8 and 9 the quantity $\int f(t,\mathbf{x},\mathbf{v})d\mathbf{x}$ at

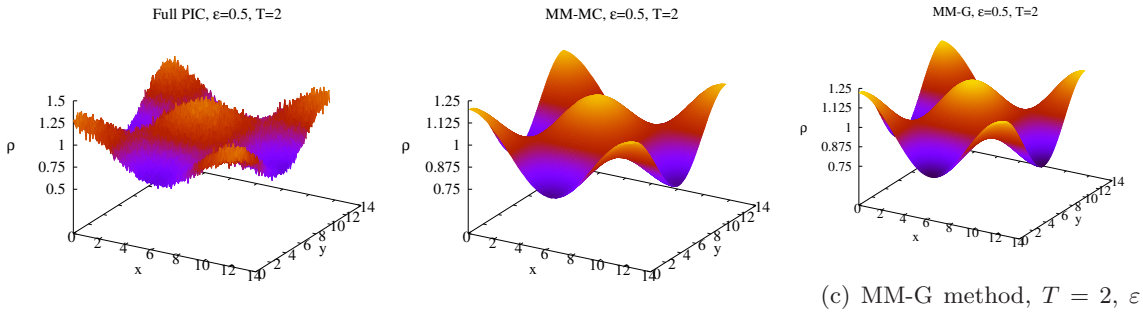

(a) Full MC, $T = 2$, $\varepsilon = 0.5$ (b) MM-MC method, $T = 2$, $\varepsilon = 0.5$ (c) MM-G method, $T = 2$, $\varepsilon = 0.5$

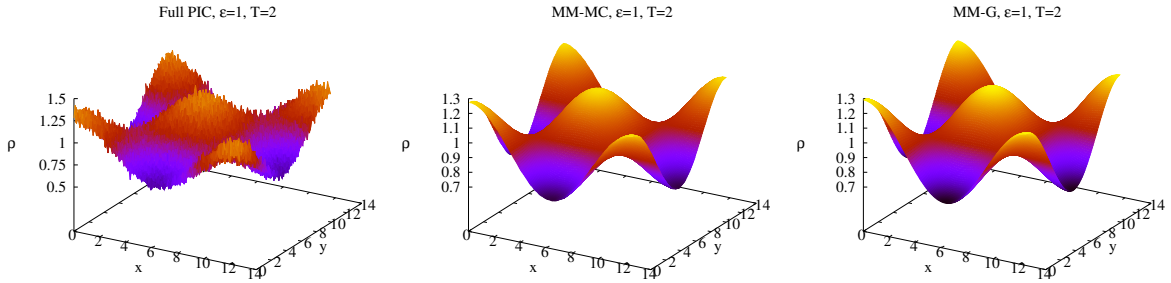

(d) Full MC, $T = 2$, $\varepsilon = 1$ (e) MM-MC method, $T = 2$, $\varepsilon = 1$ (f) MM-G method, $T = 2$, $\varepsilon = 1$

Figure 4: The density profile ρ is shown for the MM-MC, the MM-G methods and for the Full MC method in the kinetic regime.

Figure	Scheme	N_x, N_y	Typical weight	N_{v_x}, N_{v_y}	Δt	ε	T
8a, 8b, 8c, 9a, 9b,9c, 11a	MM-MC	128	5×10^{-6}		0.1	1	various
10a, 11b	MM-MC	128	5×10^{-6}		0.1	0.5	0.2
10b, 11c	MM-MC	128	5×10^{-6}		0.1	0.1	0.2
8d, 8e, 8f, 9d, 9e,9f, 11d	MM-G	128		20	0.01	1	various
10c, 11e	MM-G	128		20	0.001	0.5	0.2
10d, 11f	MM-G	128		20	0.0005	0.1	0.2

Table 3: Numerical parameters for the MM-MC and the MM-G methods non equilibrium initial data.

different times for $\varepsilon = 1$. In details, Figure 8 reports the results for the times: $T = 0$, $T = 0.2$ and $T = 0.5$ (8a, 8b and 8c for the MM-MC method, 8d, 8e and 8f for the MM-G method). Figure 9 report the results for larger times: $T = 1$, $T = 1.5$ and $T = 2$. The results given by the MM-MC method are presented in Figures 9a, 9b and 9c while for the MM-G method in 9d, 9e and 9f.

In order to see the influence of the scaling parameter ε, we also report $\int f(T, \mathbf{x}, \mathbf{v}) d\mathbf{x}$ at time $T = 0.2$ for $\varepsilon = 0.5$ in Figure 10a for the MM-MC method and in Figure 10c for the MM-G one. Moreover, the results obtained with $\varepsilon = 0.1$ by the same schemes are given in Figure 10b and in Figure 10d. Finally, in Figure 11, we compare the integral of the perturbation $\int g(T, \mathbf{x}, \mathbf{v}) d\mathbf{x}$ at $T = 0.2$ for different values of the scaling parameter ε. Results given by the MM-MC method,

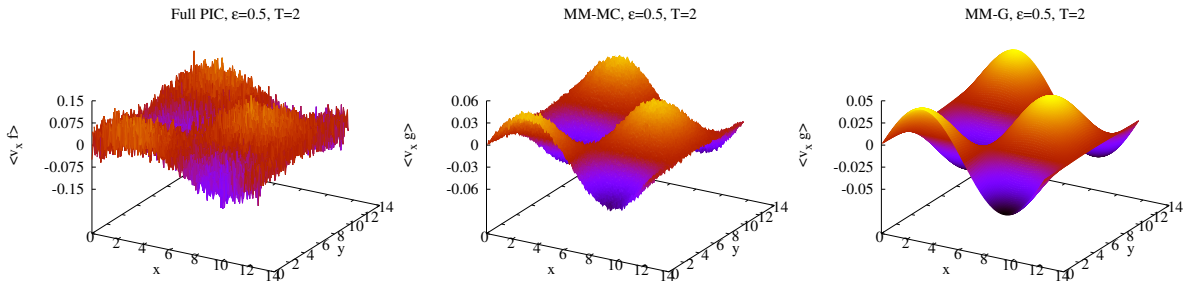

(a) Full MC, $T = 2$, $\varepsilon = 0.5$ (b) MM-MC method, $T = 2$, $\varepsilon = 0.5$ (c) MM-G method, $T = 2$, $\varepsilon = 0.5$

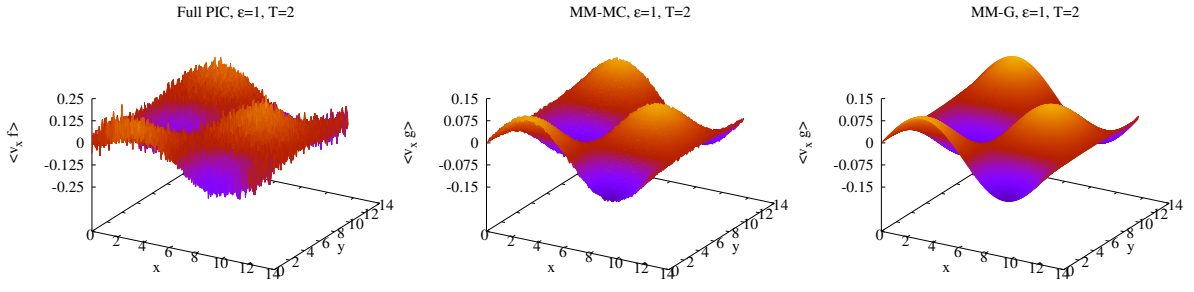

(d) Full MC, $T = 2$, $\varepsilon = 1$ (e) MM-MC method, $T = 2$, $\varepsilon = 1$ (f) MM-G method, $T = 2$, $\varepsilon = 1$

Figure 5: The component of the momentum $\langle v_x g \rangle$ (resp. $\langle v_x f \rangle$), given by the perturbation is shown for the MM-MC and the MM-G methods (resp. Full MC method), for different values of the scaling parameter ε in the kinetic regime.

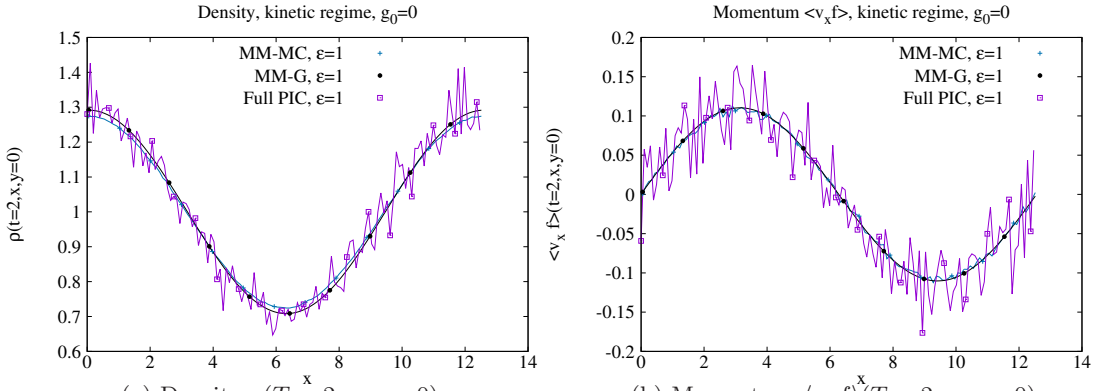

(a) Density $\rho(T = 2, x, y = 0)$ (b) Momentum $\langle v_x f \rangle (T = 2, x, y = 0)$

Figure 6: Slices of the density $\rho(T = 2, x, y = 0)$ and of the momentum $\langle v_x g \rangle (T = 2, x, y = 0)$ in the kinetic regime. Comparisons between the MM-MC, the MM-G and Full MC methods.

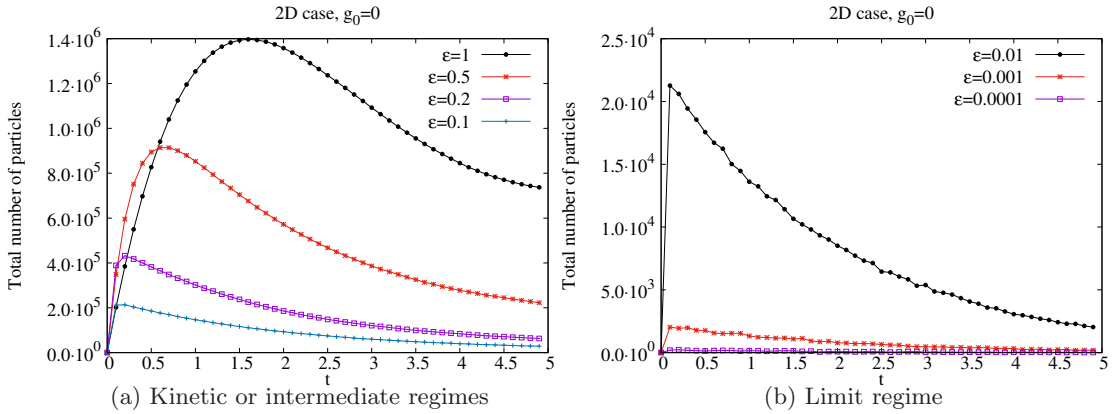

(a) Kinetic or intermediate regimes (b) Limit regime

Figure 7: Total number of particles as a function of time for a 2D-2D case with equilibrium initial condition.

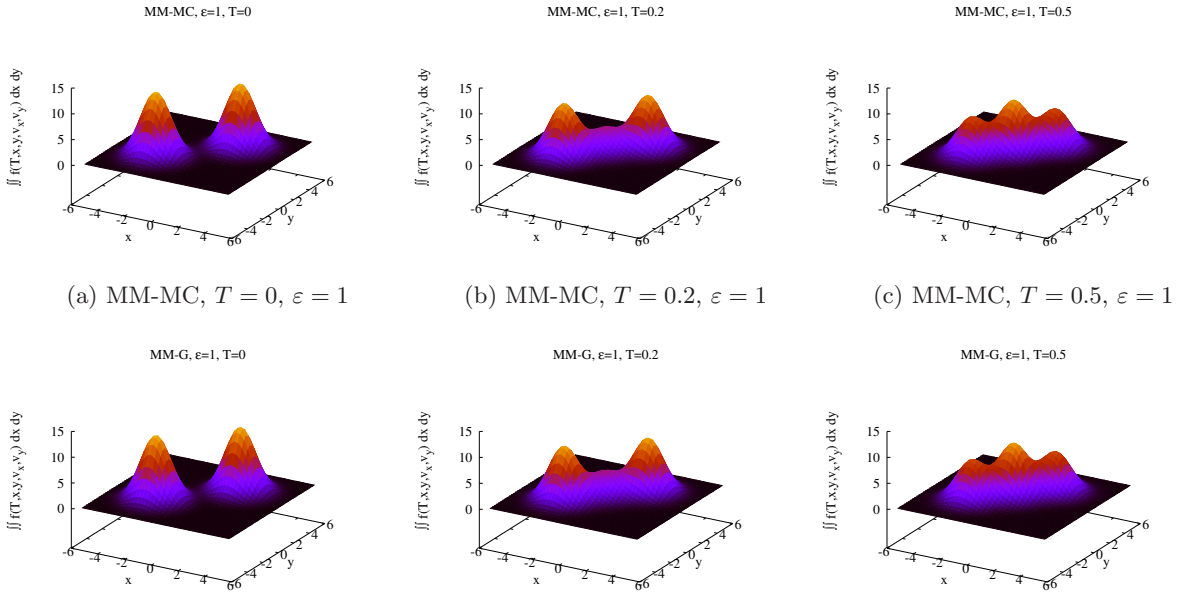

(a) MM-MC, $T = 0$, $\varepsilon = 1$ (b) MM-MC, $T = 0.2$, $\varepsilon = 1$ (c) MM-MC, $T = 0.5$, $\varepsilon = 1$

(d) MM-G, $T = 0$, $\varepsilon = 1$ (e) MM-G, $T = 0.2$, $\varepsilon = 1$ (f) MM-G, $T = 0.5$, $\varepsilon = 1$

Figure 8: Integral of the distribution function in space $\int f(T, \mathbf{x}, \mathbf{v}) d\mathbf{x}$ at times $T = 0$, $T = 0.2$ and $T = 0.5$ for $\varepsilon = 1$.

respectively the MM-G method, are presented in Figure 11a, respectively in Figure 11d, for $\varepsilon = 1$, in Figure 11b, respectively in Figure 11e, for $\varepsilon = 0.5$ and in Figure 11c, respectively in Figure 11f, for $\varepsilon = 0.1$. We summarize by observing from these test cases that the MM-MC method furnishes results which are in a very good agreement with those obtained by the reference MM-G scheme. From a computational point of view, in this situation the initial number of particles is as large as

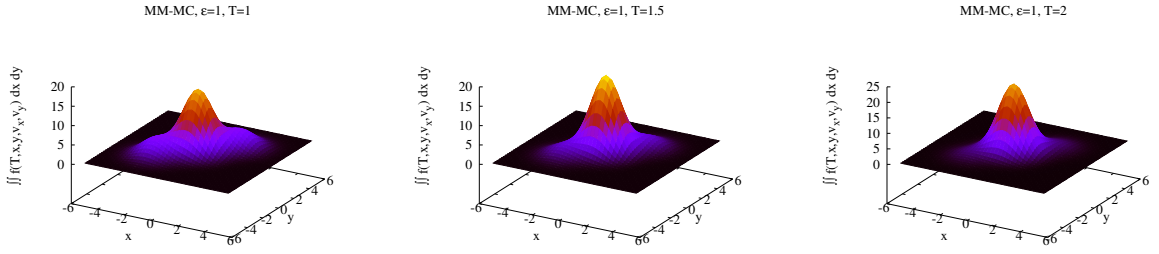

(a) MM-MC, $T = 1$, $\varepsilon = 1$ (b) MM-MC, $T = 1.5$, $\varepsilon = 1$ (c) MM-MC, $T = 2$, $\varepsilon = 1$

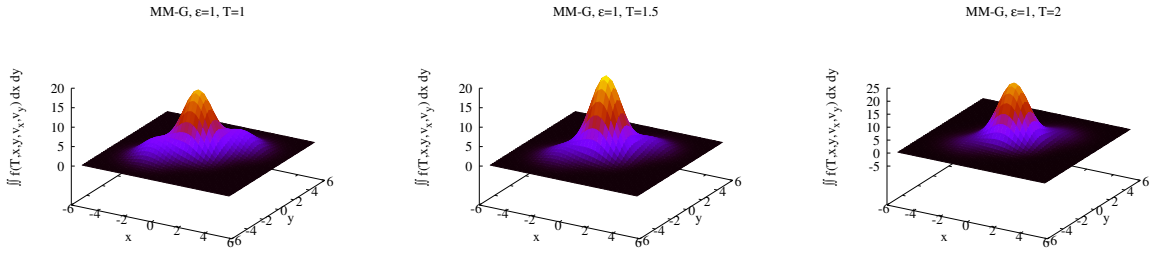

(d) MM-G, $T = 1$, $\varepsilon = 1$ (e) MM-G, $T = 1.5$, $\varepsilon = 1$ (f) MM-G, $T = 2$, $\varepsilon = 1$

Figure 9: Integral of the distribution function in space $\int f(T, \mathbf{x}, \mathbf{v}) d\mathbf{x}$ for different times $T = 1$, $T = 1.5$ and $T = 2$ and $\varepsilon = 1$.

the one used for a standard Full MC method. This is due to the fact that the initial number of particles has to be large enough to represent $g(T = 0, \mathbf{x}, \mathbf{v}) \neq 0$ with reasonable accuracy. Thus, the first iterations in time require the same computational cost as a classical full particle method. Then collisions drive the system to its equilibrium and the number of particles diminishes. We finally report the evolution in time of the number of particles for different values of ε in Figure 12: $\varepsilon = 0.1, 0.2, 0.5, 1$. The numerical parameters are: $N_x = N_y = 128$, $m_p = 5 \times 10^{-6}$ and $\Delta t = 0.1$.

4.3 Two-dimensional test cases with non constant scaling parameter

In this part, we focus on a multi-scale kinetic model where ε is now a function $\varepsilon = \varepsilon(x, y)$. The model presented in equation (1.1) is modified as follows

$$\partial_t f + \mathbf{v} \cdot \nabla_{\mathbf{x}} f = \frac{1}{\varepsilon^2(\mathbf{x})}(\rho M - f), \tag{4.21}$$

where $(\mathbf{x}, \mathbf{v}) \in [0, 4\pi]^2 \times \mathbb{R}^2$ and $t \in [0, 1]$. Periodic boundary conditions are imposed in space. We choose for $\varepsilon(\mathbf{x})$ the following shape in space

$$\varepsilon(\mathbf{x}) = 10 \left[\operatorname{atan}\Big(2(y-5)\Big) + \operatorname{atan}\Big(-2(y-5)\Big) \right] \exp\Big(-(x-10)^2 - (y-10)^2\Big) + 10^{-3}.$$

This profile is reported in Figure 13. Our Hybrid Micro-Macro Monte Carlo method is compared, as previously, to a grid based reference solution referred to as "MM-G". The latter is obtained by using the following numerical parameters: $N_x = N_y = 128$ for the spatial grid, $N_{v_x} = N_{v_y} = 32$ for

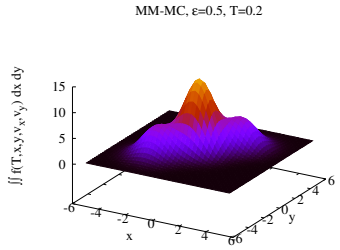

(a) MM-MC, $T = 0.2$, $\varepsilon = 0.5$

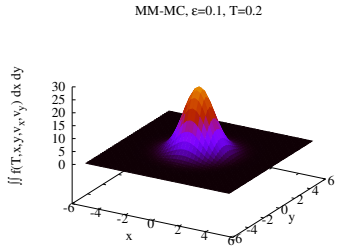

(b) MM-MC, $T = 0.2$, $\varepsilon = 0.1$

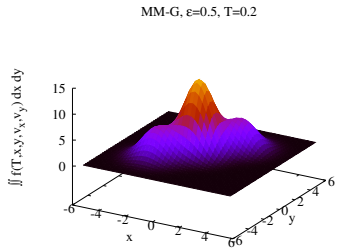

(c) MM-G, $T = 0.2$, $\varepsilon = 0.5$

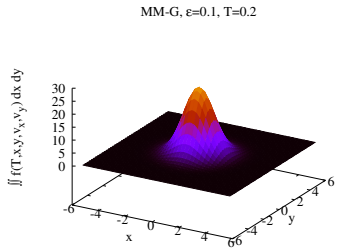

(d) MM-G, $T = 0.2$, $\varepsilon = 0.1$

Figure 10: Integral of the distribution function in space $\int f(T, \mathbf{x}, \mathbf{v}) d\mathbf{x}$ for $T = 0.2$, $\varepsilon = 0.5$ and $\varepsilon = 0.1$.

the velocity grid and $\Delta t = 10^{-4}$. As ε is small in some parts of the spatial domain, we can not use a classical full particle method for comparison. For our MM-MC solver, the numerical parameters are: $N_x = N_y = 64$, $N_p = 5000$ (hence $m_p \approx 7.7 \times 10^{-6}$), $\Delta t = 0.1$. The initial condition is chosen as

$$f_0(\mathbf{x}, \mathbf{v}) = \frac{1}{4\pi} \left[\exp\Big(- \frac{|\mathbf{v} - \mathbf{u}|^2}{2} \Big) + \exp\Big(- \frac{|\mathbf{v} + \mathbf{u}|^2}{2} \Big) \right] \rho(0, \mathbf{x}),$$

with $\mathbf{u} = (2, 2)$ and $\rho(0, \mathbf{x}) = 1 + \frac{1}{2} \cos(\frac{x}{2}) \cos(\frac{y}{2})$. In Figure 14, we plot the density at the final time $T = 1$. We observe that when ε is large, some specific structures are obtained with both solvers and solutions remain very close. This confirms the good behavior of the MM-MC method. In Figure 15, the first moment of the distribution function $\int_{\mathbb{R}^2} v_x f(T = 1, x, y_s, \mathbf{v}) d\mathbf{v}$ (with $y_s = 10, 2\pi$) is computed by the two approaches. We observe a good agreement between the grid based reference solution and our MM-MC strategy. In particular, our method is able to capture the fine kinetic effects in the zones where ε is large and diffusion is less pronounced compared to MM-G. In Figure 16 are reported the velocity repartition of the distribution functions at $\mathbf{x} = (10, 10)$ and $\mathbf{x} = (2\pi, 2\pi)$. We can observe that at the location $\mathbf{x} = (10, 10)$ (which corresponds to large values of ε), the distribution function is not in an equilibrium state whereas at $\mathbf{x} = (2\pi, 2\pi)$ (recall that $\varepsilon(2\pi, 2\pi) = 10^{-3}$), the unknown has been rapidly projected onto a Maxwellian distribution. In Figure 17, we show the distribution of the particles used to describe the perturbation g in space together with the value of ε. From the figure, it is clear that particles are automatically created in the zones in which the departure from the equilibrium state is large and are discarded in the regions in which the scaling parameter ε is small. Finally, in Figure 18, the time history of the

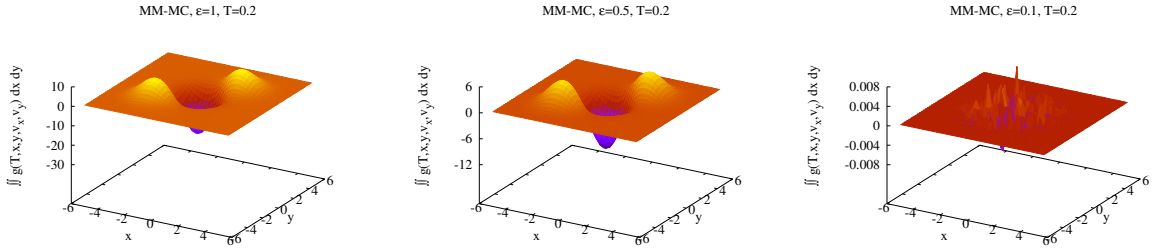

(a) MM-MC, $T = 0.2$, $\varepsilon = 1$ (b) MM-MC, $T = 0.2$, $\varepsilon = 0.5$ (c) MM-MC, $T = 0.2$, $\varepsilon = 0.1$

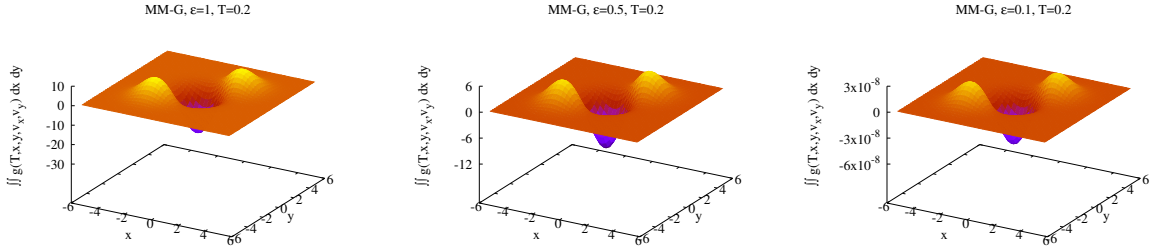

(d) MM-G, $T = 0.2$, $\varepsilon = 1$ (e) MM-G, $T = 0.2$, $\varepsilon = 0.5$ (f) MM-G, $T = 0.2$, $\varepsilon = 0.1$

Figure 11: Integral of the perturbation in space $\int g(T, \mathbf{x}, \mathbf{v}) d\mathbf{x}$ at time $T = 0.2$ for $\varepsilon = 1$, $\varepsilon = 0.5$ and $\varepsilon = 0.1$.

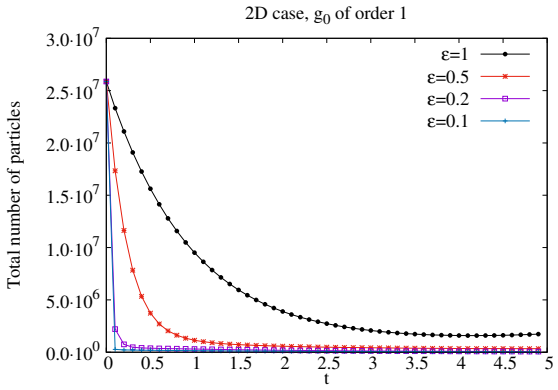

Figure 12: Total number of particles as a function of time for a non-equilibrium initial condition and different values of the scaling parameter.

number of particles is displayed. Initially, the number of particles is chosen as 5000 per cell (hence the mass of a particle is close to $m_p \approx 7.7 \times 10^{-6}$). The corresponding number of particles in the whole domain is around 3.2×10^7. After one iteration, this number is divided by 10 and decreases up to 10^6. Let us observe that the number of particles employed is a direct consequence of the magnitude of the perturbation. On the contrary a standard Monte Carlo approach would require a constant number of particles for all the simulation, which means around 15 times more particles than the one used by MM-MC method and will produce solutions with a much larger numerical

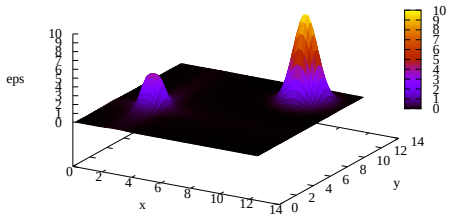

Figure 13: Profile of the scaling parameter $\varepsilon(x, y)$.

noise.

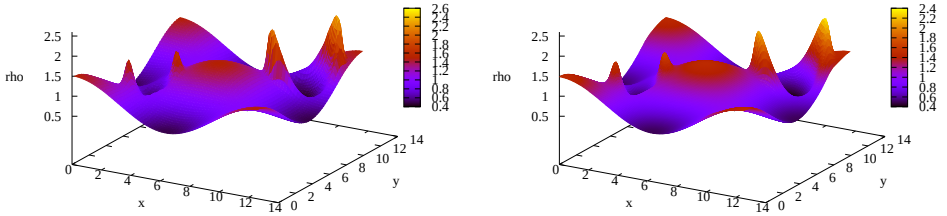

Figure 14: Density profile $\rho(T = 1, x, y)$ for the space dependent scaling parameter case. Left: MM-MC method; right: MM-G.

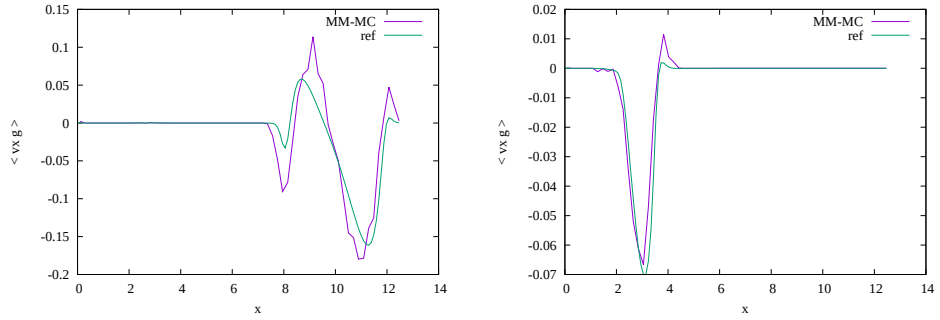

Figure 15: Slices of the momentum $\langle v_x g \rangle (T = 1, x, y = 10)$ (Left) and $\langle v_x g \rangle (T = 1, x, y = 2\pi)$ (Right) for the space dependent scaling parameter case.

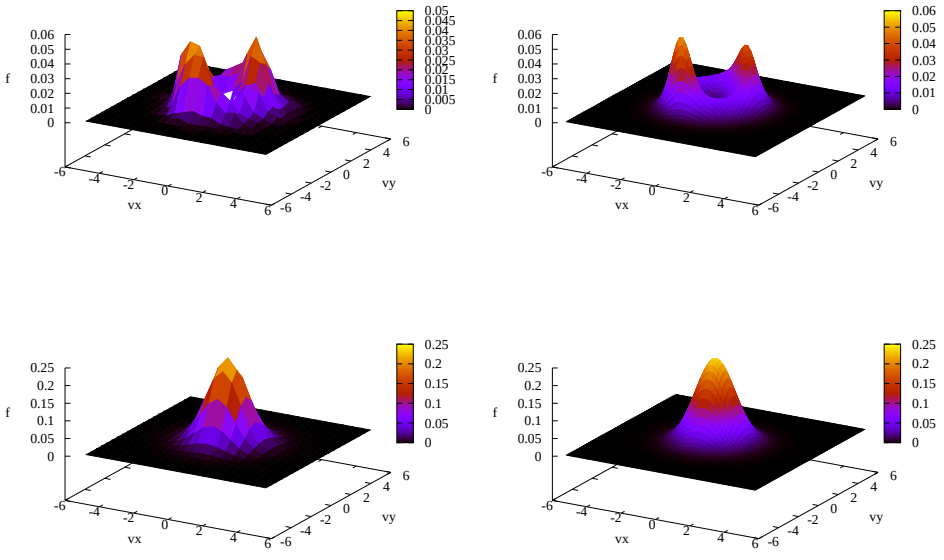

Figure 16: Velocity dependence of the distribution function at position $(x, y) = (10, 10)$ (top line) and $(x, y) = (2\pi, 2\pi)$ (bottom line) for the space dependent scaling parameter case. Left: MM-MC method; right: MM-G method.

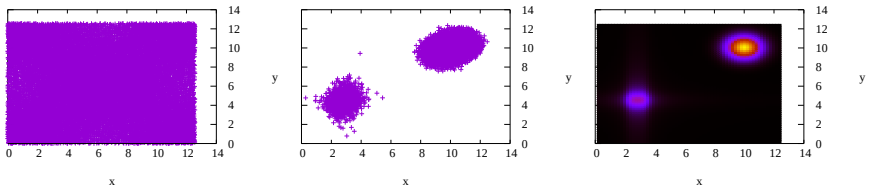

Figure 17: Localization of the particles in space for the space dependent scaling parameter case. Left: at the initial time; middle: at the final time $T = 1$; right: $\varepsilon(x, y)$.

4.4 Three-dimensional test cases

We conclude this section with a full three dimensional in space and three dimensional in velocity simulation. We consider the following initial condition

$$f_0(\mathbf{x}, \mathbf{v}) = \frac{1}{2\,(2\pi)^{3/2}} \left[\exp\Big(-\frac{|\mathbf{v} - u|^2}{2} \Big) + \exp\Big(-\frac{|\mathbf{v} + u|^2}{2} \Big) \right] \rho(0, \mathbf{x}), \tag{4.22}$$

with $u = (2, 2, 2)$ and $\rho(0, \mathbf{x}) = 1 + \frac{1}{2}\cos(\frac{x}{2})\cos(\frac{y}{2})\cos(\frac{z}{2})$ and $\mathbf{x} = (x, y, z) \in [0, 4\pi]^3$, $\mathbf{v} = (v_x, v_y, v_z) \in \mathbb{R}^3$. Periodic boundary conditions are considered in space. In this framework, we

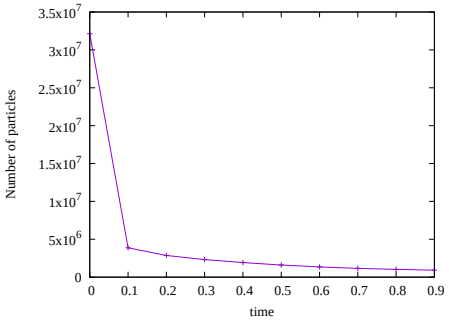

Figure 18: Time evolution of the number of particles for the space dependent scaling parameter case.

only consider our MM-MC solver, since both grid and full particle approaches are too expensive in this case. The numerical parameters of the MM-MC method are the following: $N_x = N_y = N_z = 16$, a typical weight of order 6×10^{-5}, $\Delta t = 0.1$. We present the evolution in time of the quantity $\int f(t, \mathbf{x}, \mathbf{v}) d\mathbf{x}$, obtained by our MM-MC scheme. Results obtained for $\varepsilon = 1$ are plotted in Figure 19, from $T = 0$ to $T = 1$. In Figure 20 the same diagnostic is reported for $\varepsilon = 0.1$ and $T = 0.2$, for

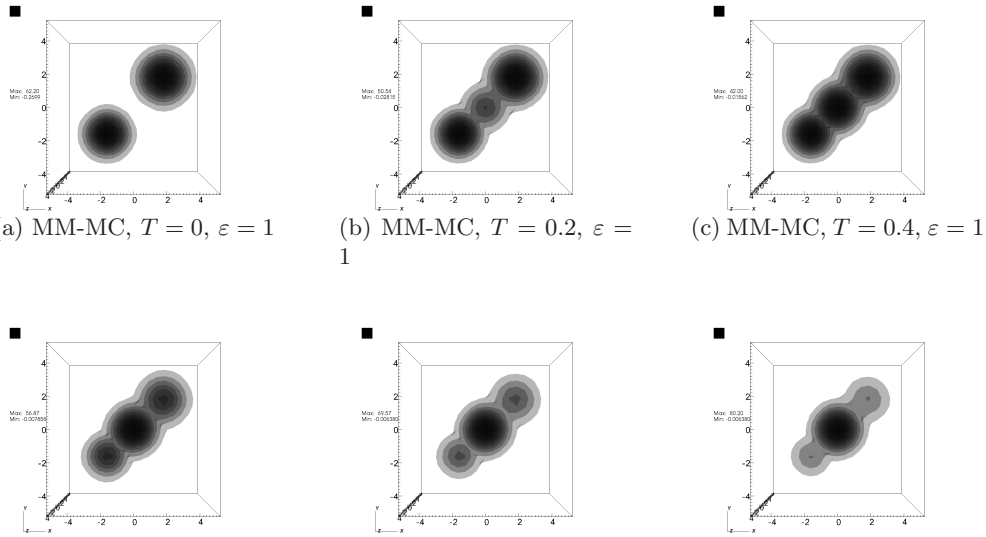

(a) MM-MC, $T = 0$, $\varepsilon = 1$ (b) MM-MC, $T = 0.2$, $\varepsilon = 1$ (c) MM-MC, $T = 0.4$, $\varepsilon = 1$

(d) MM-MC, $T = 0.6$, $\varepsilon = 1$ (e) MM-MC, $T = 0.8$, $\varepsilon = 1$ (f) MM-MC, $T = 1$, $\varepsilon = 1$

Figure 19: The integral of the distribution function in space $\int_{\mathbf{x}} f(T, \mathbf{x}, \mathbf{v}) d\mathbf{x}$ for $\varepsilon = 1$ and different times. Full three dimensional case.

$\varepsilon = 0.5$ and $T = 0.2$, and for $\varepsilon = 0.5$ and $T = 0.4$.

We finally report in Figure 21 the evolution of the number of particles in this full 3D-3D case with equilibrium initial condition

$$f(t = 0, \mathbf{x}, \mathbf{v}) = \rho(t = 0, \mathbf{x}) M(\mathbf{v}), \ \mathbf{x} \in [0, 4\pi]^3, \ \mathbf{v} \in \mathbb{R}^3,$$

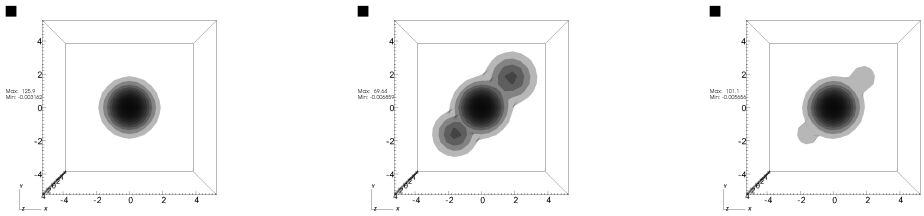

(a) MM-MC, $T = 0.2$, $\varepsilon = 0.1$ (b) MM-MC, $T = 0.2$, $\varepsilon = 0.5$ (c) MM-MC, $T = 0.4$, $\varepsilon = 0.5$

Figure 20: The integral of the distribution function in space $\int_{\mathbf{x}} f(T, \mathbf{x}, \mathbf{v}) d\mathbf{x}$ for $\varepsilon = 0.1$ and $\varepsilon = 0.5$.

with $\rho(t = 0, \mathbf{x}) = 1 + \frac{1}{2}\cos\left(\frac{x}{2}\right)\cos\left(\frac{y}{2}\right)\cos\left(\frac{z}{2}\right)$, $M(\mathbf{v}) = \frac{1}{(2\pi)^{3/2}}\exp\left(-\frac{|\mathbf{v}|^2}{2}\right)$. The space discretization is: $N_x = N_y = N_z = 16$ with a typical weight for the particles of order 5×10^{-4} and $\Delta t = 0.1$. From the results, we observe the same behaviors as for the 2D-2D case both for high values of the scaling parameter ε (Figure 21a) and in the limit regime (Figure 21b). The number of particles really employed in the construction of the solution is a function of the scaling parameter and it initially increases since the motion creates a departure from the equilibrium and successively it diminishes. This is a sign that a global equilibrium is about to be reached. In the last Figure 22,

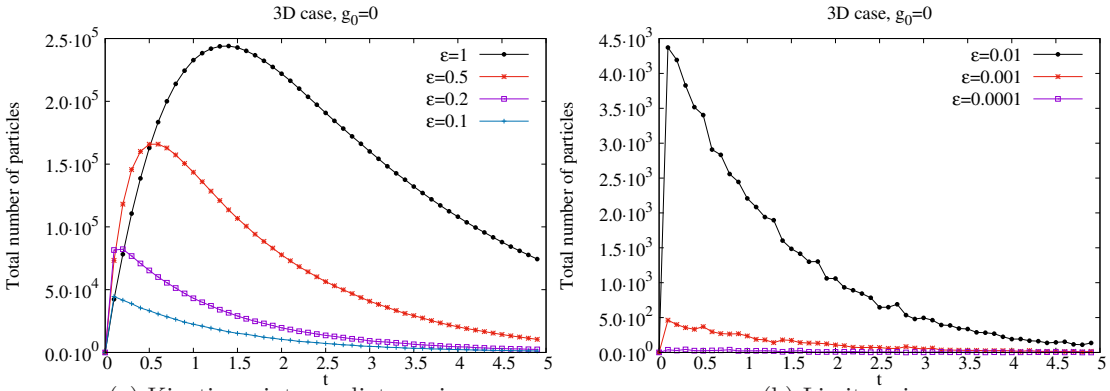

(a) Kinetic or intermediate regimes (b) Limit regime

Figure 21: Total number of particles as a function of time for the full 3D-3D case with equilibrium initial condition.

we show the evolution of the number of particles for a non-equilibrium initial condition (4.22). In this last case, the numerical parameters are $N_x = N_y = N_z = 16$, a typical weight for the particles of order 5×10^{-4} and $\Delta t = 0.1$. The same behaviors as for the 2D-2D case are observed: the number of particles used to compute the solution decreases as a function of time and as a function of the scaling parameter ε.

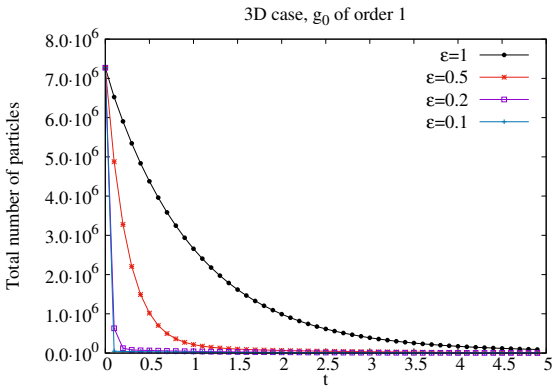

Figure 22: Total number of particles as a function of time for the full 3D-3D case with a non-equilibrium initial condition.

5 Conclusion

In this work, we have presented a new numerical method for kinetic equations in the diffusion scaling. The main lines of the proposed method are the following. (*i*) It is based on a suitable merging between Monte Carlo approach and a finite volume method. (*ii*) The Monte Carlo part of the solution is constructed to solve the perturbation part of the model while the finite volume part is designed to solve the macroscopic equilibrium part of the solution. The method enjoys some nice properties which we summarize as follows. (*a*) Compared to a standard Monte Carlo approach for solving the kinetic equation its statistical noise is smaller and it diminishes when the scaling parameter ε decreases. (*b*) It is uniformly stable with respect to the scaling parameter as well as with respect to the space mesh size. (*c*) Its computational cost as well as its variance diminish as the equilibrium is approached. (*d*) It does not need artificial transitions to pass from the microscopic description to the macroscopic one. The numerical results illustrate the efficiency of the proposed method compared to the standard Monte Carlo approaches as well as compared to standard deterministic methods based on a grid in the phase space.

In the future, we intend to work more extensively on the full three dimensional case and to consider problems with more physical relevence. In this respect, the extension of the present approach to the case of the Boltzmann operator is also under study.

Acknowledgements

N. Crouseilles and M. Lemou are supported by the French ANR project MOONRISE ANR-14-CE23-0007-01 and by the Enabling Research EUROFusion project CfP-WP14-ER-01/IPP-03. A. Crestetto is supported by the French ANR projects MoHyCon ANR-17-CE40-0027-01 and ACHYLLES ANR-14-CE25-0001.

References

[1] G. Bal, Y. Maday, *Coupling of transport and diffusion models in linear transport theory*,

M2AN Math. Model. Numer. Anal. **36**, pp. 69-86 (2002).

[2] G. Bal, L. Ryzhik, *Coupling of transport and diffusion models in linear transport theory*, SIAM, J. Appl. Math. **60**, pp. 1887-1912 (2000).

[3] M. Bennoune, M. Lemou, L. Mieussens, *Uniformly stable numerical schemes for the Boltzmann equation preserving the compressible Navier-Stokes asymptotics*, J. Comput. Phys. **227**, pp. 3781-3803 (2008).

[4] C. Bardos, F. Golse, C.D. Levermore, *Fluid dynamic limit of kinetic equations II: Convergence proofs for the Boltzmann equations*, Comm. Pure Appl. Math. **46** pp. 667-753 (1993).

[5] G.A.Bird, *Molecular gas dynamics and direct simulation of gas flows*, Clarendon Press, Oxford (1994).

[6] C.K. Birsdall, A.B. Langdon, *Plasma Physics Via Computer Simulation*, Institute of Physics (IOP), Series in Plasma Physics (2004).

[7] S. Boscarino, L. Pareschi, G. Russo, *Implicit-Explicit Runge-Kutta schemes for hyperbolic systems and kinetic equations in the diffusion limit*, J. Sci. Comp. **35**, pp. 22-51 (2013).

[8] S. Boscarino, L. Pareschi, G. Russo, *A unified IMEX Runge-Kutta approach for hyperbolic systems with multiscale relaxation* , SIAM J. Num. Anal. **55**, pp. 2085-2109 (2017).

[9] C. Buet, S. Cordier, *Asymptotic preserving scheme and numerical methods for radiative hydrodynamic models*, Comptes Rendus Mathématique **338**, pp. 951-956 (2004).

[10] K.M. Case, P.F. Zweifel, Linear Transport Theory, Addison-Wesley, Reading, MA, (1967).

[11] S. Chandrasekhar, Radiative Transfer, Dover, New York, (1960).

[12] R. E. Caflisch, *Monte Carlo and Quasi-Monte Carlo Methods*, Acta Numerica pp. 1–49 (1998).

[13] C. Cercignani, *The Boltzmann equation and its applications*, Springer Varlag New York, (1988).

[14] A. Crestetto, N. Crouseilles, M. Lemou, *Kinetic/Fluid micro-macro numerical schemes for Vlasov-Poisson-BGK equations using particles*, Kin. Rel. Models **5**, pp. 787-816 (2012).

[15] A. Crestetto, N. Crouseilles, M. Lemou, *A particle micro-macro decomposition based numerical scheme for collisional kinetic equations in the diffusion scaling*, accepted in Communications in Mathematical Sciences (2018).

[16] N. Crouseilles, G. Dimarco, M. Lemou, *Asymptotic preserving and time diminishing schemes for rarefied gas dynamic*, Kinetic and Related Models **10**, pp. 643-668 (2017).

[17] N. Crouseilles, M. Lemou, *An asymptotic preserving scheme based on a micro-macro decomposition for collisional Vlasov equations: diffusion and high-field scaling limits*, Kin. Rel. Models **4**, pp. 441-477 (2011).

[18] P. Degond, G. Dimarco, *Fluid simulations with localized Boltzmann upscaling by Direct Simulation Monte-Carlo*, J. Comput. Phys. **231**, pp. 2414-2437 (2012).

[19] P. Degond, G. Dimarco, L. Mieussens, *A multiscale kinetic-fluid solver with dynamic localization of kinetic effects*, J. Comp. Phys., **229** pp. 4907–4933 (2010).

[20] P. Degond, G. Dimarco, L. Pareschi, *The moment guided Monte Carlo method*, Int. J. Num. Meth. Fluids **67**, pp. 189-213 (2011).

[21] P. Degond, S. Jin, *A smooth transition model between kinetic and diffusion equations*, J. Num. Anal. **42** pp. 2671–2687 (2005).

[22] G. Dimarco, L. Pareschi, *Hybrid multiscale methods II. Kinetic equations*, SIAM Multiscale Modeling and Simulation **6** pp. 1169-1197 (2007).

[23] G. Dimarco, L. Pareschi, *A Fluid Solver Independent Hybrid method for multiscale kinetic equations*, SIAM J. Sci. Comput. **32** pp. 603-634 (2010).

[24] G. Dimarco, L. Pareschi, *Numerical methods for kinetic equations*, ACTA Numerica, **23**, pp. 369-520 (2014).

[25] G. Dimarco, L. Pareschi, G. Samaey, *Asymptotic Preserving Monte Carlo methods for transport equations in the diffusive limit*, SIAM J. Sci. Comput. **40** pp. A504-A528, (2018).

[26] F. Filbet, T. Rey, *A hierarchy of hybrid numerical methods for multi-scale kinetic equations*, SIAM J. Sci. Comput. **37** pp A1218-A1247, (2015).

[27] F. Golse, S. Jin, C. D. Levermore, *A domain decomposition analysis for a two-scale linear transport problem*, Mathematical Modelling and Numerical Analysis **37**, pp. 869-892 (2003).

[28] S. Jin, *Efficient Asymptotic-Preserving (AP) schemes for some multiscale kinetic equations*, SIAM J. Sci. Comput. **21**, pp. 441-454 (1999).

[29] S. Jin, L. Pareschi, G. Toscani, *Uniformly accurate diffusive relaxation schemes for multiscale transport equations*, SIAM J. Numerical Analysis **38**, pp. 913-936, (2000).

[30] S. Jin, X. Yang, F. Golse, Z.Y. Huang, *Numerical study of a domain decomposition method for a two-scale linear transport equation*, Networks and Heterogeneous Media **1**, pp. 143-166 (2006).

[31] A. Klar, *An asymptotic-induced scheme for non stationary transport equations in the diffusive limit*, SIAM Journal of Numerical Analysis **35**, pp. 1073-1094 (1998).

[32] A. Klar, *Asymptotic induced domain decomposition methods for kinetic and drift diffusion semiconductor equations*, SIAM J. Sci. Comp. **19**, pp. 2032-2050 (1998).

[33] A. Klar, *A numerical method for kinetic semiconductor equations in the drift diffusion limit*, J. Sci. Comp. **19** pp. 2032–2050 (1998).

[34] A. Klar, H. Neunzert, J. Struckmeier, *Transition from kinetic theory to macroscopic fluid equations: a problem for domain decomposition and a source for new algorithms*, TTSP **29**, pp. 93-106 (2000).

[35] A. Klar, N. Siedow, *Boundary layers and domain decomposition for radiative heat transfer and diffusion equations: applications to glass manufacturing processes*, Eur. J. Appl. Math. **9**, pp. 351-372 (1998).

[36] K. Krycki, C. Berthon, M. Frank, R. Turpault, *Asymptotic preserving numerical schemes for a nonclassical radiation transport model for atmospheric clouds*, Math. Meth. Applied Scie. **36**, pp. 2101-2116 (2013).

[37] P. Lafitte, G. Samaey, *Asymptotic-preserving projective integration schemes for kinetic equations in the diffusion limit*, SIAM J. Sci. Comp. **34** pp. A579–A602 (2012).

[38] S. Liu, Monte Carlo strategies in scientific computing, Springer, (2004).

[39] E. W. Larsen, J. B. Keller, *Asymptotic solution of neutron transport problems for small mean free paths*, J. Math. Phys, **15** pp. 75-81 (1974).

[40] M. Lemou, *Relaxed micro-macro schemes for kinetic equations*, Comptes Rendus Mathématique **348**, pp. 455-460 (2010).

[41] M. Lemou, F. Méhats, *Micro-macro schemes for kinetic equations including boundary layers*, SIAM J. Sci. Comput. **34**, pp. 734-760 (2012).

[42] M. Lemou, L. Mieussens, *A new asymptotic preserving scheme based on micro-macro formulation for linear kinetic equations in the diffusion limit*, SIAM J. Sci. Comp. **31**, pp. 334-368 (2008).

[43] P. Le Tallec, F. Mallinger, *Coupling Boltzmann and Navier-Stokes by half-fluxes*, J. Comput. Phys. **136**, pp. 51-67 (1997).

[44] T.-P. Liu, S.-H. Yu, *Boltzmann equation: micro-macro decompositions and positivity of shock profiles*, Comm. Math. Phys. **246**, pp. 133-179 (2004).

[45] P. Markowich, *The Stationary Semiconductor Device Equations*, Springer-Verlag, (1986).

[46] G. Naldi, L. Pareschi, *Numerical schemes for kinetic equations in diffusive regimes*, Applied Math. Letters **11**, pp. 29-35, (1998).

[47] D. W. Peaceman, H. H. Rachford, *The numerical solution of parabolic and elliptic differential equations*, Journal of the Society for Industrial and Applied Mathematics **3**, pp. 28-41 (1955).

[48] W. Ren, H. Liu, S. Jin, *An Asymptotic-Preserving Monte Carlo method for the Boltzmann equation*, J. Comp. Phys. **276**, pp. 380-404 (2014).

[49] P. Sharma, G. Hammett, *A fast semi-implicit method for anisotropic diffusion*, J. Comput. Phys. **230**, pp. 4899-4909 (2011).

[50] S. Tiwari, A. Klar, S. Hardt, *A particle-particle hybrid method for kinetic and continuous equations*, J. Comput. Phys. **228**, pp. 7109-7124 (2009).

[51] T. Xiong, J. Qiu, *A Hierarchical Uniformly High Order DG-IMEX Scheme for the 1D BGK Equation*, J. Comput. Phys. **336**, pp. 164-191 (2017).